bioRxiv preprint doi: https://doi.org/10.1101/206086; this version posted October 19, 2017. The copyright holder for this preprint (which was not certified by peer review) is the author/funder, who has granted bioRxiv a license to display the preprint in perpetuity. It is made available under aCC-BY-NC-ND 4.0 International license.

Temporal metacognition as the decoding of self-generated brain dynamics

Tadeusz W. Kononowicz[1*], Clemence Roger[2], Virginie van Wassenhove[1*]

[1] Cognitive Neuroimaging Unit, CEA DRF/Joliot, INSERM, Université Paris-Sud, Université Paris-Saclay, NeuroSpin center, 91191 Gif/Yvette, France; [2] Université de Lille, CNRS, UMR 9193 - SCALab - Sciences Cognitives et Sciences Affectives, F-59000 Lille, France
[*] Corresponding author

Tadeusz W. Kononowicz
Tel.: +33(0)1.69.08.79.38
CEA/DRF NeuroSpin - INSERM Cognitive Neuroimaging Unit
Bât 145 Point Courrier 156
Gif s/ Yvette F-91191 FRANCE
t.w.kononowicz@icloud.com

Virginie van Wassenhove
Virginie.van.Wassenhove@gmail.com

ABSTRACT (150 words)

Metacognition, the ability to know about one's thought process, is self-referential. Here, we studied the brain mechanisms underlying metacognitive inferences in a self-generated behavior. Human participants generated a time interval, and evaluated the signed magnitude of their timing (first and second order behavioral judgments, respectively) while being recorded with time-resolved neuroimaging. We show that the first- and second-order judgments relied on the power of beta oscillations (β; 15-40 Hz), while error monitoring subsystems engaged alpha oscillations (α; 8-14 Hz). The spread of an individual's β power state-space trajectories during timing was indicative of the individual's metacognitive inference. Our results suggest that network inhibition (β power) instantiates a state variable determining future network trajectory; this naturally provides a code for duration and metacognitive inferences would consist in reading out this state variable. Altogether, our study describes oscillatory mechanisms for timing suggesting that temporal metacognition relies on inferential processes of self-generated dynamics.

AUTHOR CONTRIBUTIONS

V.W., C.R., and T.W.K. designed the research. C.R. and T.W.K. performed the experiments. T.W.K. and V.W. analyzed the data. T.W.K. and V.W. wrote the manuscript.

ACKNOWLEDGMENTS

This work was supported by an ERC-YStG-263584 and an ANR10JCJC-1904 to V.vW. We thank the members of UNIACT and the medical staff at NeuroSpin for their help in recruiting and scheduling participants. We thank members of UNICOG for fruitful discussions. Preliminary data were presented at SFN (2012, Washington DC), and SFN (2015, Washington DC). We thank four anonymous reviewers for the depth and incisiveness of their comments.

bioRxiv preprint doi: https://doi.org/10.1101/206086; this version posted October 19, 2017. The copyright holder for this preprint (which was not certified by peer review) is the author/funder, who has granted bioRxiv a license to display the preprint in perpetuity. It is made available under aCC-BY-NC-ND 4.0 International license.

INTRODUCTION

A central question in cognitive neuroscience is how humans evaluate and self-monitor their cognitive states, a generic ability referred to as metacognition (Fleming & Dolan, 2012). In daily life, self-monitoring and action evaluation typically involve some form of time estimation, from appropriate turn taking during conversations to sophisticated movement timing when creating enjoyable artistic expressions. Surprisingly however, theories of psychological time do not account for time monitoring abilities despite early work suggesting their implication in metacognition (Miltner et al., 1997). By far, only one observation in animals (Meck et al., 1984) and one behavioral study in humans (Akdogan & Balci, 2017) have reported the ability to self-monitor and to rate confidence in decision-making during time estimation, respectively. We will refer to (temporal) metacognition in humans as the intelligible inference of one's magnitude estimation – measured herein through temporal production. Here, we asked to which extent temporal metacognition can be reliable during time estimation, and which neural indices may dissociate the self-generation of a time interval (first order judgment, FOJ) from the self-assessment of the produced time interval (second order judgment, SOJ).

To address these questions, human participants were asked to produce time intervals and, *post factum*, to self-estimate the signed error magnitude of their time production, *i.e.*, to evaluate whether they were shorter or longer than the required target duration (**Fig. 1**). In this temporal production task, participants were required to initiate a time interval by button press followed by a second button press after they considered that 1.45 s had elapsed. Hence, participants had full volitional control over their time production in the absence of any sensory cues. Additionally, participants could solely rely on their self-generated internal dynamics coding for the target duration both, for their time production, and for their metacognitive assessment (FOJ and SOJ, respectively). This design enabled to address the possibility of internal timing or duration being explicitly available to awareness through self-referential metacognition (Block, 1995; Fleming et al., 2012). Because current neuroscientific models posit that internal dynamics in timing are mediated by oscillatory or state-dependent network dynamics (Laje & Buonomano, 2013; Karmarkar & Buonomano, 2007; Buhusi & Meck, 2005; Merchant et al., 2013; Allman et al., 2014; Gu et al., 2015; van Wassenhove, 2016; Bueno et al., 2017), we combined magneto- and electroencephalography (M/EEG) to quantify the dynamics of oscillatory brain responses when participants engaged in self-generated and self-assessed timing.

Using a temporal production task to assess metacognition provided several paradigmatic and conceptual benefits. First, the requirements of a temporal production task may capitalize on forward-inverse models posited in motor execution (Miall & Wolpert, 1998): here, the key variable for the motor goal would be the timing of the second button press given *when* the first button press was made. This internal state variable could be used forward in the elicitation of a ballistic motor trajectory for the execution of the second button press, thereby allowing the minimization of execution errors (Harris & Wolpert, 1998) in time. Second, the availability of an internal variable coding for the target duration could provide useful information regarding the uncertainty or noise level of the motor timing goal (Harris & Wolpert, 1998), which, in turn, could be

bioRxiv preprint doi: https://doi.org/10.1101/206086; this version posted October 19, 2017. The copyright holder for this preprint (which was not certified by peer review) is the author/funder, who has granted bioRxiv a license to display the preprint in perpetuity. It is made available under aCC-BY-NC-ND 4.0 International license.

utilized for metacognitive assessment. In this context, a parsimonious hypothesis was that the neural markers of the internal timing variable would support both FOJ and SOJ. In agreement with a two-staged process in time estimation (van Wassenhove, 2009), an internal variable coding for duration would be set forth in the brain, and decoding the current-state (*via* reverse-inference) would help establish temporal meta-representations. Our experimental approach also differed from previous metacognitive tasks in at least two important ways. A majority of studies investigating second order metacognitive inferences have focused on the role of sensory evidence in driving confidence, and used rewards that were contingent on sensory stimuli being smaller or larger than an imposed categorical boundary (Bogacz et al., 2006; Gold & Shadlen, 2007). Here, the task fully relied on internal variables in the absence of sensory-driven confidence. Additionally, metacognitive inferences consisted in indicating the *signed magnitude* of timing-errors in the produced duration unlike a recent temporal error monitoring approach (Akdogan & Balci, 2017) in which participants categorically estimated their confidence in making a temporal judgment. We also provided participants with an unlimited decision time to prevent the tendency of fast and error-prone decisions.

In this study, we report that participants can reliably estimate the direction and the magnitude of their errors prior to receiving any feedback on the validity of their produced time interval. These results confirmed the ability to detect and estimate one's temporal errors during time production. Second, we describe several neural markers tracking participants' first and second order judgments. In particular, our results suggest that the power of beta (β) oscillations may indicate the internal state variable posited to code for duration in FOJ. The second order inferences (SOJ) were non-linearly related to the β power coding for FOJ. We also report that the distance in β state-space could inform on the reliability of an individual's metacognitive inferences. Finally, alpha (α) power in distinct brain regions correlated with FOJ and SOJ after time estimation, indicating parallel analyses of FOJ and SOJ likely based on the β state-dependent networks. Altogether, our findings provide novel evidence for the neural signatures of self-referential awareness in time estimation.

Portions of these results have been presented at conferences (C. Roger, M. Buiatti, V. van Wassenhove, *Soc. Neurosci. Abstr.* 2012-S-8620, 2012; H. Tajuddin, T.W. Kononowicz, C. Roger, V. van Wassenhove, *Soc. Neurosci. Abstr.* 439.21, 2015), and other group have recently showed metacognitive effects in line with our current report. Nevertheless, their task and conclusions based on psychophysical and computational approaches are very different from the magneto- and electro-physiological approaches presented here, and the conceptual insights they provide.

bioRxiv preprint doi: https://doi.org/10.1101/206086; this version posted October 19, 2017. The copyright holder for this preprint (which was not certified by peer review) is the author/funder, who has granted bioRxiv a license to display the preprint in perpetuity. It is made available under aCC-BY-NC-ND 4.0 International license.

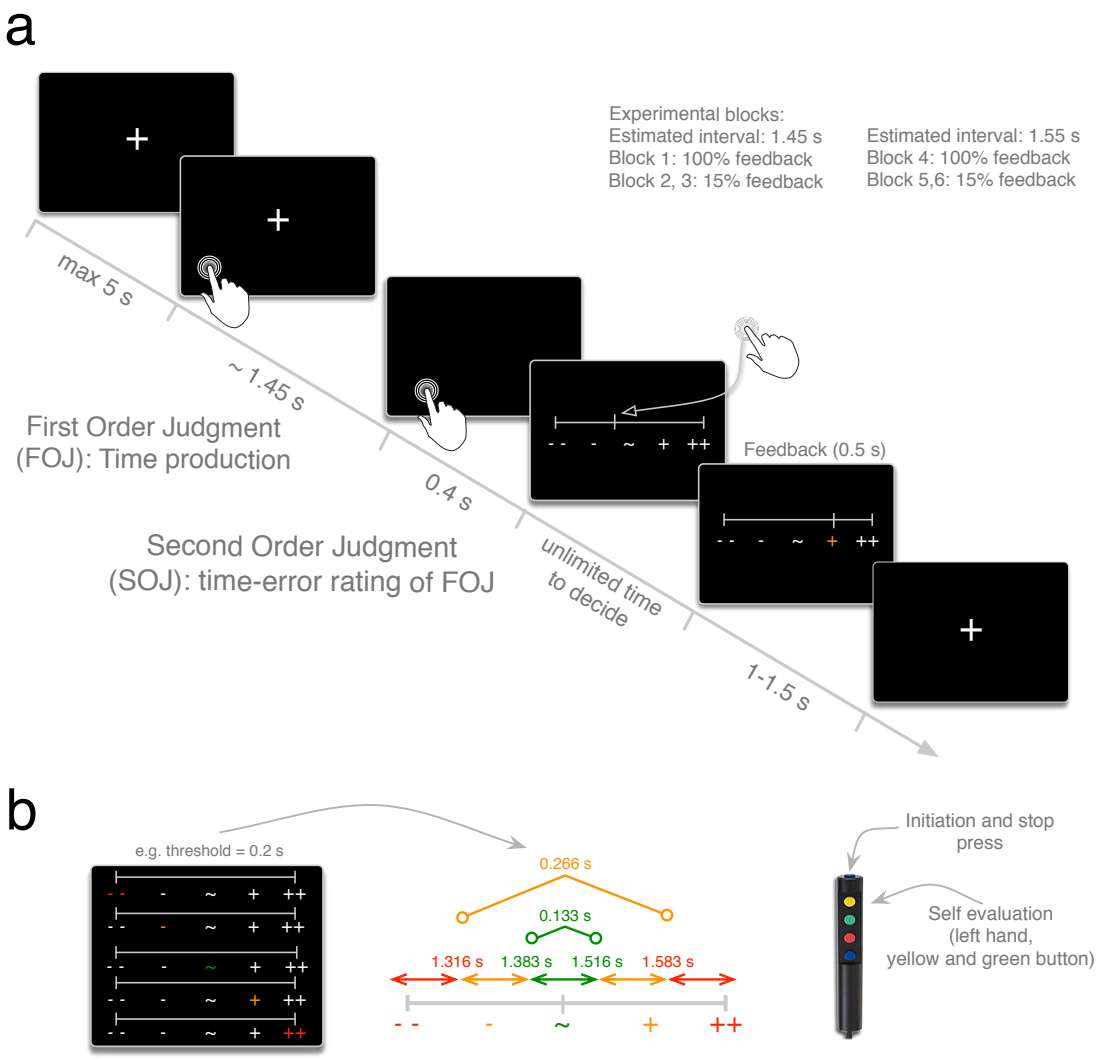

Figure 1. Experimental paradigm. (**a**) Time course of an experimental trial. (**b**) Scale for participants' self-assessment and feedback. Feedback categories were individually tailored according to individuals' duration discrimination threshold (green: correct category; yellow: slightly shorter or longer; red: too short or too long). The right panel illustrates the response mapping for SOJ.

RESULTS

We first provide behavioral evidence showing that participants can accurately perform a temporal FOJ and retrospectively access its precision with a SOJ. We then quantify oscillatory signatures of the FOJ, and explore to which extent they may serve metacognitive inferences (SOJ). We also explore typical markers of time related processes and error-monitoring (contingent negative variation, CNV and error related negativity, ERN, respectively). Our analytical approach uses statistical modeling of single-trial data and dimensionality reduction methods for M/EEG data.

Drifting time production (FOJ) over time with no loss of precision

In the course of the experiment, participants (n = 12) accurately produced the 1.45 s target interval (Blocks 1-3) and the adjusted 1.56 s intervals (Blocks 4-6: feedback was implicitly and individually adjusted

bioRxiv preprint doi: https://doi.org/10.1101/206086; this version posted October 19, 2017. The copyright holder for this preprint (which was not certified by peer review) is the author/funder, who has granted bioRxiv a license to display the preprint in perpetuity. It is made available under aCC-BY-NC-ND 4.0 International license.

to a new target value; cf. Methods) as depicted in the density function over FOJ (**Fig. 2a**). Moreover, as can be seen in **Fig. 2b,** the increase of FOJ was steady and progressive over the course of the entire experiment. Given the task structure, the consecutive changes in feedback and implicit duration co-occurred with the unexpected drift of participants' duration estimation: specifically, in the 100% feedback blocks (Blocks 1 and 4), both time intervals were accurately produced with a mean of 1.490 s and 1.582 s, respectively (**Fig. 2a**); in the 15% feedback blocks (Blocks 2, 3 and 5, 6), the length of the FOJ significantly increased (**Fig. 2a**; dashed lines). In these 15% feedback blocks, participants' temporal productions were significantly longer for both the 1.45 s target interval (**Fig 2a**; $F(8.0) = 11.3$, $p > 10^{-15}$; + 90 ms on average) and the 1.56 s adjusted interval ($F(7.6) = 10.4$, $p > 10^{-15}$; + 78 ms). This suggested a natural tendency of participants to lengthen their time estimates over time when less feedback was provided: however, the blocks providing less feedback systematically occurred after the 100% feedback blocks. Although for both the 1.45s and 1.56s time intervals, the amount of feedback was the only factor to be warranted in the models containing the intercept (1.45 s target: $\Delta AIC = 123$, $\chi^2(1.0) = 6084832$, $p > 10^{-15}$; adjusted 1.56 s interval: $\Delta AIC = 104$, $\chi^2(0.9) = 4500629$, $p > 10^{-15}$), we could not disentangle with full certainty the time-on-task effect of consecutive blocks, and the specific feedback effects.

Nevertheless, some patterns suggested that the amount of feedback was not the main contributor to the observed drift in time estimation (**Fig 2b**). For instance, to assess the possibility of a step-like transition between Block 3 (explicit 1.45s target) and 4 (implicit adjusted 1.56s target), we used the last 10 trials of Block 3 and the first 10 trials of Block 4. The transition trials from Block 3 and 4 did not significantly differ (**Fig. 2c**; $F(1) = 0.6$, $p > 0.1$) suggesting no clear behavioral transition when the feedback was implicitly changed, even when provided on every single trial (Block 4). Given the lengthening of FOJ, we also tested whether the precision of time production changed in the course of the experiment. If so, this would indicate that participants may not perform the task with consistent focus over time, or may change their strategy when feedback was implicitly changed. For this, we measured the coefficients of variation (CVs, variance divided by the mean) per block, and interestingly found that, in spite of the drift, the precision of FOJ did not significantly differ across blocks as tested by repeated measures ANOVA ($F(5, 65) = 0.9$, $p > 0.1$). This demonstrated the stability of behavioral precision throughout the experiment, and indicated that participants were performing the task as required.

It is thus noteworthy that despite not explicitly informing participants about the change in target duration introduced in Blocks 4, 5, and 6, participants readily adjusted their temporal production (FOJ) without any loss in the precision of their temporal production (**Fig. 2c**). This observation suggests that humans can implicitly monitor their temporal criterion as was previously shown in rats (Meck et al., 1984).

We then asked whether humans could explicitly monitor such internal criterion explicitly, as recent work would suggest (Akdogan & Balci, 2017), by asking participants to introspect about their produced duration (SOJ). Due to the progressive lengthening of FOJ across experimental blocks, the behavioral data were z-scored separately for each block to allow exploiting and analyzing the local variations in single-trial estimates without any confounding influence of time-on-task effects.

bioRxiv preprint doi: https://doi.org/10.1101/206086; this version posted October 19, 2017. The copyright holder for this preprint (which was not certified by peer review) is the author/funder, who has granted bioRxiv a license to display the preprint in perpetuity. It is made available under aCC-BY-NC-ND 4.0 International license.

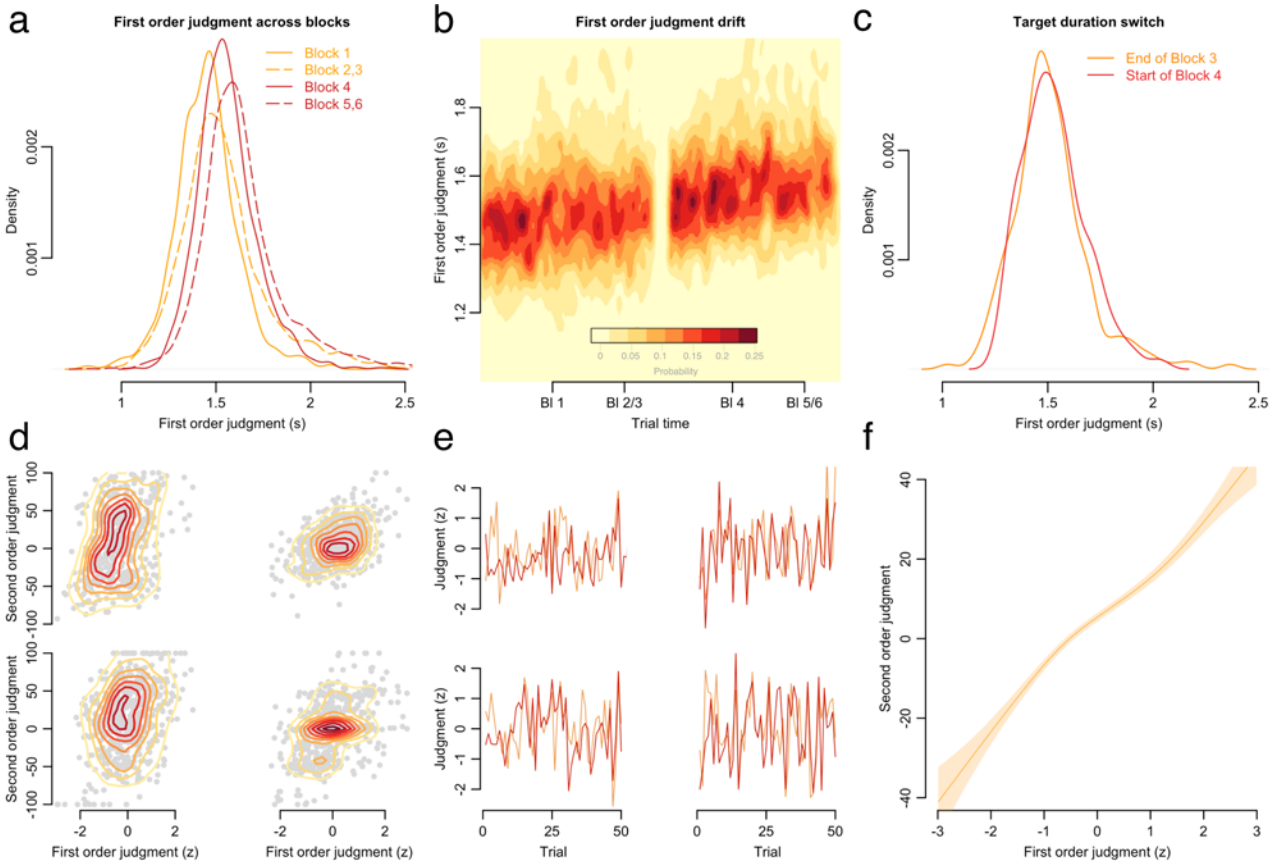

Figure 2. Behavioral evidence for temporal production (FOJ) and temporal metacognition (SOJ). (**a**) Probability density function of all participants' time productions separately for each experimental block. Yellow is 1.45 s; red is 1.55 s. (**b**) Continuous density plot of duration productions in the course of the whole experiment. Red values indicate the distribution of time production for all participants (n=12) throughout all experimental blocks. The yellow break indicates the transition between Block 3 and 4. (**c**) Probability density functions of the last 10 trials in Block 3 and the first 10 trials in Block 4, computed across individual trials for all participants. (**d**) Raw data of four participants illustrating SOJ as a function of FOJ in a two dimensional density plot marked by the isometric lines. (**e**) The four participants' first 50 experimental trials were z-scored for easier visualization: SOJ (orange) tracked FOJ (red) over time. (**f**) The regression line is the GAMM model fit between SOJ and FOJ estimates for all participants.

Behavioral evidence for metacognitive inference in time estimation

Individuals could estimate and track their FOJ over time (**Fig. 2d, e**, respectively). To understand how precisely participants could self-estimate their temporal productions, we assessed whether the SOJ predicted the performance during FOJ on a single-trial basis using a generalized mixed model approach. We found that FOJ and SOJ were strongly correlated on a trial-by-trial basis (**Fig. 2f**, $F(4.0) = 192.5$, $edf = 4.0$, $p < 10^{-15}$), suggesting that participants could correctly assess the signed error magnitude of their just produced time interval. Additionally, the model fit revealed a nonlinearity in the regression slope between FOJ and SOJ (**Fig. 2f**). The nonlinear term was modeled using a flexible nonlinear spline term provided by GAMM (cf. Methods) and was compared to the model allowing only linear terms ($\Delta AIC = 15.5$, $\chi^2(4.6) = 18576$, $p < 0.001$). This nonlinearity indicated that the correlation was slightly less steep for the FOJ intervals close to the target duration, and steeper for FOJ away from the target duration. This pattern indicated that temporal productions (FOJ) closest to the internal target duration criterion were harder to self-estimate (SOJ). This intuitive pattern will also be observed later on in brain activity.

bioRxiv preprint doi: https://doi.org/10.1101/206086; this version posted October 19, 2017. The copyright holder for this preprint (which was not certified by peer review) is the author/funder, who has granted bioRxiv a license to display the preprint in perpetuity. It is made available under aCC-BY-NC-ND 4.0 International license.

We then asked whether this SOJ effect was driven by a sequential effect due to feedback delivered on the previous trial. To test this, we fitted the model adding the factor 'FOJ on n-1 trial' as a fixed effect. The analysis was constrained to blocks with 100% feedback (Block 1 and 4) so that all trials - but the first one - were effectively preceded by feedback. The model comparison showed a marginal trend towards an n-1 duration effect (ΔAIC = 0.9, $\chi^2(1.0) = 2135$, $p = 0.091$), suggesting that the longer the previous FOJ was, the shorter the current SOJ tended to be ($F(1.0) = 2.9$, $edf = 1.0$, $p = 0.09$). The trend towards sequential effect in duration production was suggestive of implicit monitoring in humans in line with previous studies (Meck et al., 1984; Meck 1988) showing that rats' anticipatory behavior was negatively correlated with response times in the previous trial. Nevertheless, on a trial-by-trial basis, the strongest statistical relationship we observed was between FOJ and SOJ ($F(1.0) = 293.2$, $edf = 1.0$, $p < 10^{-15}$), suggesting that human participants most exclusively based their self-estimation (SOJ) on the current trial estimation.

Although unlikely given the experimental instructions, an additional scenario accounting for the interaction between FOJ and SOJ was that participants intentionally increased the variance of their temporal productions (FOJ) improve their self-assessment (SOJ). This cognitive strategy would confound the possibility of an internal state variable being monitored, and this possibility was not controlled for in previous work (Akdogan & Balci, 2017). To address this important issue, we performed a control experiment in which we manipulated the incentives: participants produced 1.45 s durations, and either received points for their FOJ accuracy in one block (**Supplementary Fig. 1a**) or for the congruence between their FOJ and their SOJ in another block (**Supplementary Fig. 1a**). If participants used the confounding strategy described above, the regression slope for FOJ and SOJ should be significantly larger in the congruence incentive condition than in the FOJ accuracy incentive condition. In this control experiment, the FOJ significantly covaried with SOJ (**Supplementary Fig. 1a**; $F(1.0) = 76.0$, $edf = 1.0$, $p < 10^{-15}$) just as we observed in our main experimental design. Most importantly, the addition of the block type factor was not justified in the model (ΔAIC = 1.9, $\chi^2(1) = 1.7$, $p > 0.1$), demonstrating that participants performed the task sequentially by first estimating FOJ and then estimating SOJ without alternative cognitive strategies. To further strengthen the observations in the control experiment, we checked whether the spread of FOJ estimations could account for an individual's metacognitive inference. Individual differences in metacognitive inference (FOJ*SOJ) were not correlated with the individuals' coefficient of variation observed in FOJ (**Supplementary Fig. 1b**, *rho* = 0.08; $p = 0.81$). This observation did not support the idea that participants boost their FOJ and SOJ correlation, but rather that participants effectively complied with the original task goal of inferring the magnitudes of their temporal errors following their temporal productions.

One last confounding factor regarding the existence of reliable SOJ in temporal estimation could be the uncertainty associated with the timing process itself. Specifically, the width of diffusion of an unknown number of accumulators could be used for metacognitive inference as opposed to timing *per se* (Akdogan & Balci, 2017). In our task, this hypothesis would predict that the speed of decision-making in SOJ (measured as reaction times) should significantly differ as a function of the magnitude of the SOJ. To test this, we fitted a model in which FOJ and SOJ were entered as predictors for reaction times on a given trial: neither FOJ nor SOJ terms were significant (all $p > 0.1$). Thus, we found no evidence that decision speed covaried with FOJ

bioRxiv preprint doi: https://doi.org/10.1101/206086; this version posted October 19, 2017. The copyright holder for this preprint (which was not certified by peer review) is the author/funder, who has granted bioRxiv a license to display the preprint in perpetuity. It is made available under aCC-BY-NC-ND 4.0 International license.

or with SOJ. Participants did not seem to use chronometric uncertainties to reach their decision for their metacognitive inference, suggesting that the second order decision in our task could be a readout of the FOJ motor timing goal. This operation would be conceptually and computationally very different from a second order decision established on the certainty of temporal error (Akdogan & Balci, 2017) as will be commented in the Discussion section.

To sum up, our behavioral findings indicated that participants produced temporal targets with overall constant precision in the course of the experiment, and that timing errors during temporal production could be accessed through metacognitive inference. We then tested the working hypothesis that the neural markers of the internal variable coding for the target duration may support both first and second order judgments. For this, we analyzed the M/EEG data recorded while participant underwent the behavioral task.

β power as a signature state variable for FOJ

We first explored the implication of known timing-related signatures such as slow activity (Contingent Negative Variation, CNV (Kononowicz & Penney, 2016; Macar & Vidal, 2004) and *β* power (Kononowicz & Van Rijn, 2015; Kulashekar et al., 2016) in FOJ. Using all sensors over the interval ranging from 0.4 s to 1.2 s following the first button press, we found no significant differences in the amplitude of the slow evoked responses as a function of duration estimation (all $p > 0.1$, **Supplementary Fig. 2a**). This replicated previous work discussing the functional implication of slow activity in timing (Kononowicz & Van Rijn, 2011, Kononowicz & Van Rijn, 2014). In the same time window (0.4 to 1.2 s), we instead observed that longer produced durations showed a significant cluster of larger β power in both EEG and MEG data ($p = 0.020$, **Fig. 3a; Supplementary Fig. 2bc**). To prevent binning FOJ data according to performance, which could be considered somewhat arbitrary, we also used FOJ as a continuous predictor in a Generalized Additive Mixed Model (Wood, 2017; GAMM), which could accommodate nonlinear predictors and interactions: this analysis confirmed that longer durations elicited larger β power in a large cluster of sensors (**Fig. 3b**, **Supplementary Table 1**). The bilateral motor and midline cortices were the likeliest generators for the β power changes as a function of duration production (**Fig. 3a**). No other oscillatory responses showed significant changes as a function of temporal production (FOJ, $p > 0.1$).

Crucially, duration production did not correlate with EMG activity (**Supplementary Fig. 3,** $p > 0.1$) or with duration press (measured between the button press and its release) ($p > 0.1$, GAMM), thereby excluding the contribution of low-level factors to the β power effect which could have confounded the role of β oscillations in time estimation in previous work (Kononowicz & Van Rijn, 2015).

Nevertheless, one possibility was that β power was directly related to motor preparation, and not to timing *per se*. For instance, previous research has shown that changes in β power correlated with latency changes caused by the directional uncertainty of motor responses (Tzagarakis, et al., 2010). Here, no changes in direction were necessary as both button presses were identical, and no other variables than internal timing was required by the task. An alternative hypothesis was that β power changes were a marker of a drift-like

bioRxiv preprint doi: https://doi.org/10.1101/206086; this version posted October 19, 2017. The copyright holder for this preprint (which was not certified by peer review) is the author/funder, who has granted bioRxiv a license to display the preprint in perpetuity. It is made available under aCC-BY-NC-ND 4.0 International license.

accumulation so that the peak latency of β power *preceding* the second button press would differ across produced durations. Such latency differences would predict that, at a given latency near the second button press, β power would significantly differ across produced timing. To test this hypothesis, we fitted the GAMM to the mean values of β power locked to the second button press (0.4 s before the second button press). None of the fitted model terms were significant after FDR correction in either MEG or EEG (e.g. **Supplementary Fig. 4** for EEG), providing no substantial evidence for the contribution of motor preparation or accumulation-like processes in the fluctuations of β power.

Across many studies (e.g., Kononowicz & Van Rijn, 2015; Meijer et al., 2016), β power can readily be seen at a stable latency of roughly ~500 ms following the onset of the timed interval as also observed here following the first button press. A plausible and parsimonious way to reconcile seemingly disparate findings would be to posit that the internal state variable for timing in motor execution always contributes to the uncertainty in motor execution. This would be consistent with reports of β power in motor execution tasks (Tan et al., 2016), the more specific observations that β power fluctuates according to uncertainty and predictability in motor timing (Meijer et al., 2016; Tzagarakis, et al., 2010) and, more generally, in many explicit motor timing tasks (e.g. Fujioka et al, 2012). Altogether, our results replicate and strengthen the implication of β oscillations in duration estimation (Kononowicz & Van Rijn, 2015; Kulashekar et al., 2016) and their possible instantiation as a state variable indicative of the motor timing goal. Our and others' results would thus be consistent with the notion that a state-dependent variable for timing can be initiated after the start of a time interval, and β power appears a good predictor of the subsequent length of the time interval.

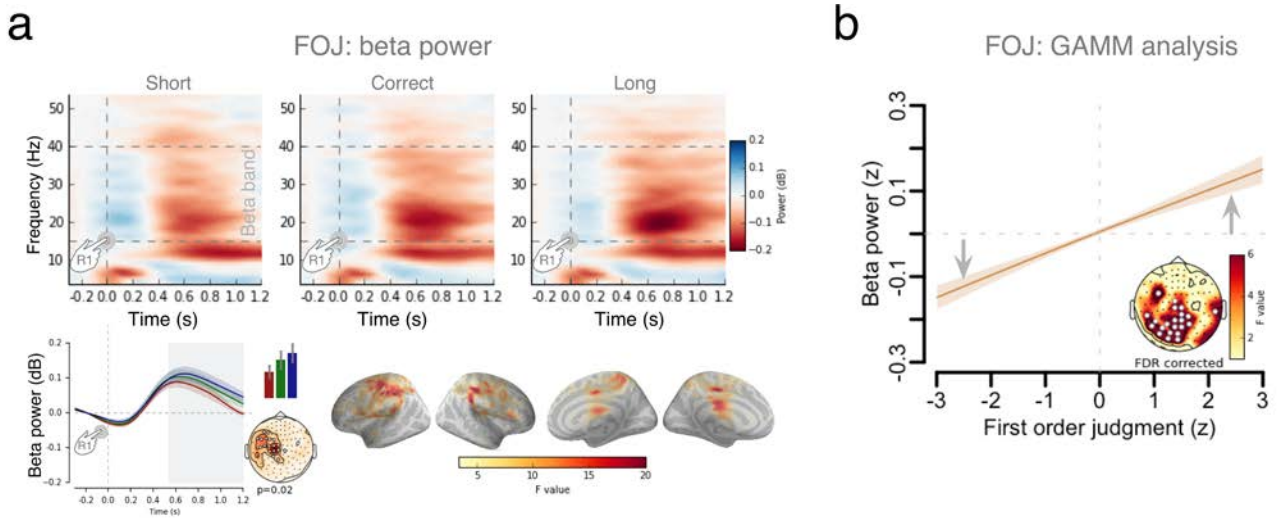

Figure 3. β power as a signature state variable for FOJ. Time-frequency spectrum for the example sensor. β power time courses sorted as a function of FOJ categories found in the sensor with the highest F-value. The β band is demarcated by the horizontal dotted lines. Below, a time-based cluster permutation t-test for the frequencies (15-40 Hz) shows latencies (grayed) at which β power significantly differed across conditions. The bar plot provides the average β power over the time window in the topographical cluster. Source estimates contrasting FOJ driven β power effects are also illustrated (uncorrected F-map) and reveal the implication of medial and motor regions. (**b**) Regression plot showing that β power covaries with FOJ (GAMM model fit). The topographical map shows the distribution of significant sensors. Statistical details are in **Supplementary Table 1**. The arrows indicate that the effect is driven by a departure of the z-scored β values away from their mean value.

bioRxiv preprint doi: https://doi.org/10.1101/206086; this version posted October 19, 2017. The copyright holder for this preprint (which was not certified by peer review) is the author/funder, who has granted bioRxiv a license to display the preprint in perpetuity. It is made available under aCC-BY-NC-ND 4.0 International license.

Non-linear use of β power for metacognitive inference

One working hypothesis was that the availability of an internal variable coding for duration may be shared by both FOJ and SOJ. Hence, the next question was whether β power also varied as a function of SOJ. The analysis of oscillatory power in the same time window showed no significant clusters, whether splitting SOJ in categories (**Supplementary Fig. 5,** all $p > 0.1$) or using SOJ as a continuous predictor in a GAMM ($p > 0.1$). Although β power did not directly correlate with SOJ, metacognitive inferences may still rely on β power by means of establishing the difference between the β power indicating the length of the produced time interval, and the actually produced interval. To address this possibility, we defined a neural congruence score between FOJ and SOJ, which consisted of the absolute difference of z-scored β power in single-trials FOJ and SOJ. This congruence score was meant to capture the distance of an individual's SOJ from the individual's temporal production (FOJ) so that high Congruence indicated that the SOJ matched the FOJ. The sign of the congruence score was captured by the interaction between FOJ and SOJ.

The full GAMM model allowing non-linear terms had the following specification: β *power* ~ *FOJ* + *SOJ* + *Congruence* + *FOJ*SOJ* + *FOJ*Congruence*. FOJ, SOJ, and other predictors were entered as continuous variables (cf. Methods). Although the main term Congruence, and the interaction between FOJ and SOJ showed no significant clusters, the interaction between FOJ and Congruence revealed a significant change of β *power* in selected sensors (**Fig. 4**, **right panel**, **Supplementary Table 2**). Specifically, the model comparison showed a significant nonlinear interaction between FOJ and Congruence when compared to the model without the interaction term (**Fig. 4**; $\Delta AIC = 14.0$ $\chi^2(2.1) = 9.6$, $p < 0.001$). The 3D plot and the heat map illustrate that for high Congruence scores, the power of β oscillations strongly predicted the FOJ. This effect could be seen in the increase of β power from point 'b' to point 'c' in the 'congruent' part of the surface (**Fig. 4, left panel**). This indicated that when participants correctly self-estimated their temporal production, β power was also predictive of FOJ. As the Congruence score decreased towards point 'a' in the plot (**Fig. 4, left panel**), the predictive power of β for FOJ also decreased. In sum, the use of GAMM allowed us to show that β power was non-linearly related to SOJ with increased β power for trials in which participants provided an accurate metacognitive inference on their temporal production, *i.e.*, when participants were aware of the direction and the magnitude of their time errors. This pattern was consistent with the non-linearities reported in the behavioral results.

As β power appeared to spread according to the produced duration, we hypothesized that the more distant beta power was from the planned target duration, the better metacognitive judgments might be on a per individual basis – as also suggested in behavioral data (**Fig. 2f**) in which SOJ closest to the FOJ were harder to self-estimate. To test this hypothesis, we decomposed the β power into latent components using dPCA method (Machens, 2010; Kobak et al., 2016) and quantified the distance in β state-space as a function of FOJ and SOJ.

bioRxiv preprint doi: https://doi.org/10.1101/206086; this version posted October 19, 2017. The copyright holder for this preprint (which was not certified by peer review) is the author/funder, who has granted bioRxiv a license to display the preprint in perpetuity. It is made available under aCC-BY-NC-ND 4.0 International license.

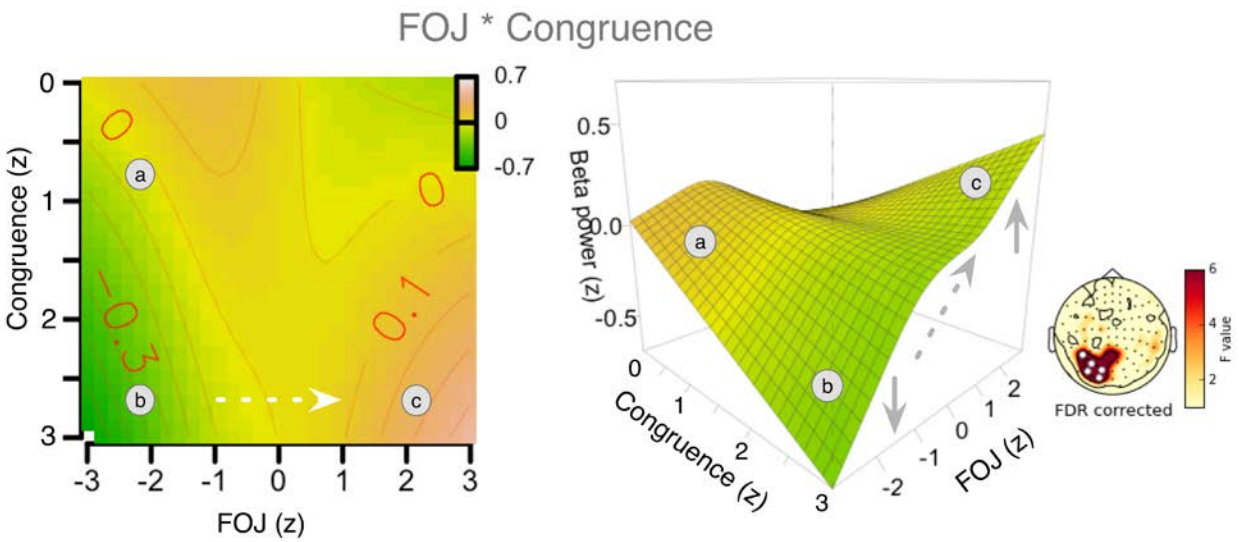

Figure 4. Use β power for metacognitive inference. The results of GAMM model fit for the interaction term between FOJ and Congruence. The analysis of Congruence score indicated that β power was a strong predictor of FOJ for Congruent trials when FOJ matched SOJ judgments. For these Congruent trials, strong differences between β power values for duration of different lengths may have been used retrospectively to judge FOJ. Statistical details in **Supplementary Table 2**.

Distance in β state space predicts metacognitive inference

We quantified metacognitive inference as the correlation (Spearman's *rho*) between FOJ and SOJ on a per individual basis. To avoid an arbitrary topographic selection of sensors we employed two methods to obtain distance in β state space driven by the FOJ split.

First, we quantified the grand average power in each frequency band for each individual and across all sensors in order to decompose brain activity into latent components with the dPCA method (Machens, 2010; Kobak et al., 2016). Although the dPCA method was originally designed for cell population analyses in a single cortical region, we used it here across sensors, with sensors somewhat homologous to a population of neurons with mixed selectivities. Specifically, we looked at the morphology of the two first demixed Principal Components (dPC; cf. Methods) which showed that β power rose fast at the onset of the FOJ and remained segregated in different locations of the neural state-space corresponding to the 'short', 'correct', and 'long' FOJ (**Fig. 5a**). This pattern was found for nearly all participants in the study as depicted in **Fig. 5a** and the separation is illustrated for participant 1 in **Fig. 5b**.

Next, we conservatively quantified the multidimensional distance in β power state-space between FOJ ('short', 'correct', 'long') as a function of the individual's metacognitive inference (FOJ*SOJ), *i.e.* we computed the Spearman's *rho* correlation between FOJ and SOJ on a per individual basis. We found a significant correlation between an individual's SOJ and the distance between FOJ conditions in the defined β state-space ($rho = 0.75$, $p = 0.005$; **Fig. 5b**). This result indicated that the larger the distance between the FOJ, the better the SOJ were. Importantly, the multidimensional distance in β state-space was not driven by the spread of individual FOJ responses, quantified by Coefficient of Variation (CV-FOJ; standard deviation of an individual's FOJ divided by its mean) ($rho = 0.26$, $p = 0.42$; **Supplementary Fig. 6a**). To further insure that

bioRxiv preprint doi: https://doi.org/10.1101/206086; this version posted October 19, 2017. The copyright holder for this preprint (which was not certified by peer review) is the author/funder, who has granted bioRxiv a license to display the preprint in perpetuity. It is made available under aCC-BY-NC-ND 4.0 International license.

there was no confound with the behavioral variance in CV-FOJ, we computed robust linear regressions: a comparison of the null model to the model containing β power was justified ($F_{robust} = 8.0$, $p = 0.004$) whereas the inclusion of CV-FOJ against the null model was not warranted ($F_{robust} = 0.03$, $p = 0.9$) demonstrating that including the CV-FOJ did not significantly account for the variance in the model. CV-FOJ and dPC1 were also dissociated as the model containing CV-FOJ and dPC1 was preferred over the model containing only CV ($F_{robust} = 7.3$, $p = 0.006$).

The dissociation between CV-FOJ and dPC1 showed that the distance in β state-space was not solely driven by inter-individual variability in FOJ, but rather, by timing. No other frequency bands or components were significant (all $p > 0.1$; **Supplementary Fig. 6bc**). To strengthen the outcomes of the dPCA analysis, we also quantified the Euclidean distance in β power separately, for each sensor. With this method, the estimated distance in β space for a cluster of sensors was significantly correlated with metacognitive inference (**Fig. 5c**, white topographic dots).

We thus showed that the larger the distance in β state space (using dPCA or directly computing Euclidean distances of β power), the more accurate the metacognitive inference on a per individual basis. For instance, the individuals framed in blue (**Fig. 5c**) showed a much large spread of their beta state-space (**Fig. 5a**) and higher metacognitive inference (**Fig. 5c**). Conversely, the individuals framed in red (**Fig. 5c**) showed a much smaller spread of their beta state-space (**Fig. 5a**) and lower metacognitive inference (**Fig. 5c**). Our β state-space analysis provided strong evidence that the distance in β state-space could serve temporal metacognition by providing a second order estimation of FOJ. The distance in β state-space may thus reflect the individual degree of metacognitive inference, akin to reading-out β power retrospectively.

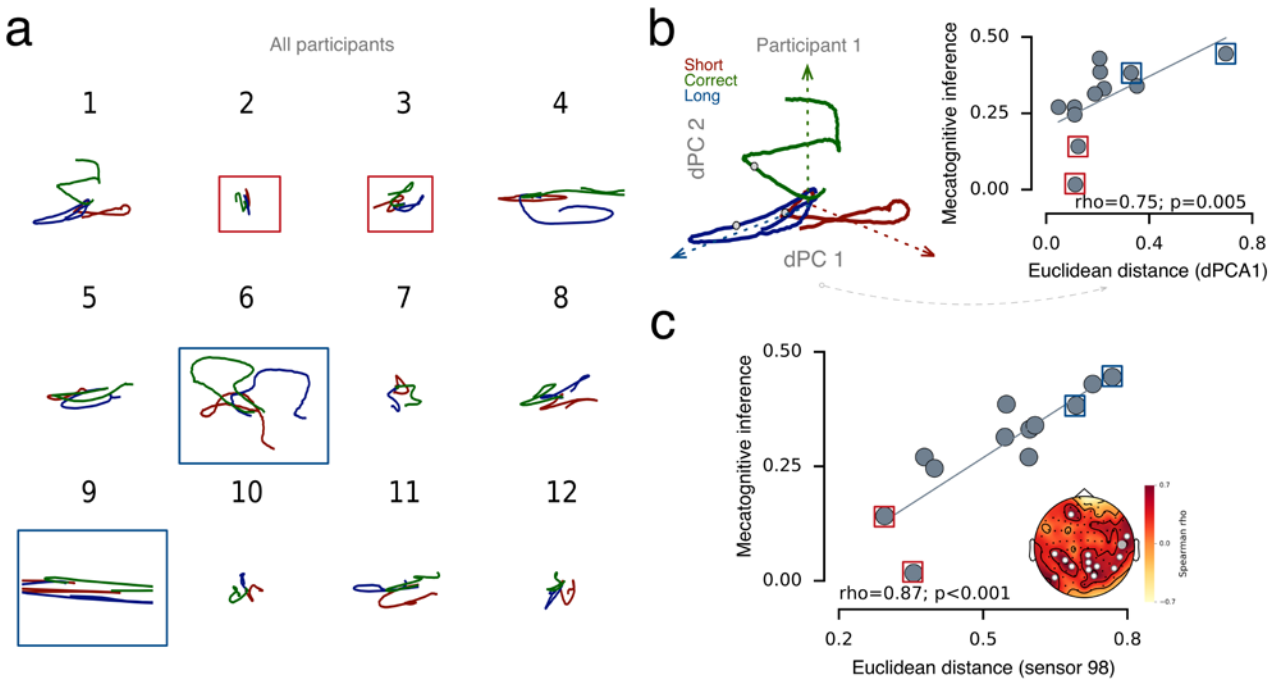

Figure 5. Distance in β state space supports metacognitive inference. (**a**) Individual outcomes of dPCA analyses. (**b**) dPCA decomposition in β band illustrated for one participant (left panel). The two first dPCs are displayed against each other, following typical state-space analysis, and illustrating an early path separation. Gray marks indicate the 200 ms time point, after which the activity reached a stable attractor state. The correlation plot illustrates individual distances in

bioRxiv preprint doi: https://doi.org/10.1101/206086; this version posted October 19, 2017. The copyright holder for this preprint (which was not certified by peer review) is the author/funder, who has granted bioRxiv a license to display the preprint in perpetuity. It is made available under aCC-BY-NC-ND 4.0 International license.

β state space (dPC 1) against metacognitive inference (FOJ*SOJ) showing significant correlations. Red and blue rectangles correspond to trajectories in panel 'a', highlighting examples of participants with low and high metacognitive inference ability, respectively. (**c**) The correlation plot illustrates individual distances in β space plotted against metacognitive inference. The plot displays a sensor with the most significant correlation, marked as blue in the topographical plot. The topographical plot displays the distribution of sensors where distance in β power was correlated with metacognitive inference.

Sustained activity as signature of SOJ readout

If such β power readout for SOJ occurred retrospectively, it may also be time-locked to the moment at which participants decided to make their second button press in order to terminate the planned time interval. At roughly 200 ms preceding a movement, recent findings (Schultze-Kraft et al., 2016) have demonstrated that participants could not veto their decision to move. Here, this signifies that information relevant to the outcome of the temporal production task may be available for the SOJ, and thus that this time period may contribute to SOJ. To assess this possibility, evoked activity was locked to the second keypress in order to look at the amplitude of the evoked brain responses preceding (-0.4 to 0 s) the second button press. We found significant differences in the amplitude of the evoked activity as a function of SOJ (**Fig. 6a**) by considering SOJ as a continuous factor using GAMM (**Fig. 6b**). Specifically, we observed a positive frontal cluster (**Fig. 6b**, **Supplementary Table 3**) that covaried negatively with SOJ (**Fig. 6b**) (and a posterior negative cluster that co-varied positively with SOJ; **Fig. 6b**, **Supplementary Table 4**). In line with this bipolar EEG scalp distribution, and in agreement with previous work (Wiener et al., 2010), the brain sources at the origin of this activity were located in the motor, the premotor and the mid-frontal regions (**Fig. 6c**). These results indicate that the SOJ of temporal production was available prior to the second button press has been made. However, as FOJ contribution to slow activity was not relevant, the whole process may signify some initial stages of readout in which first order information becomes available after termination of the second button press. Therefore, we had a closer look at the post interval signatures of temporal error-monitoring.

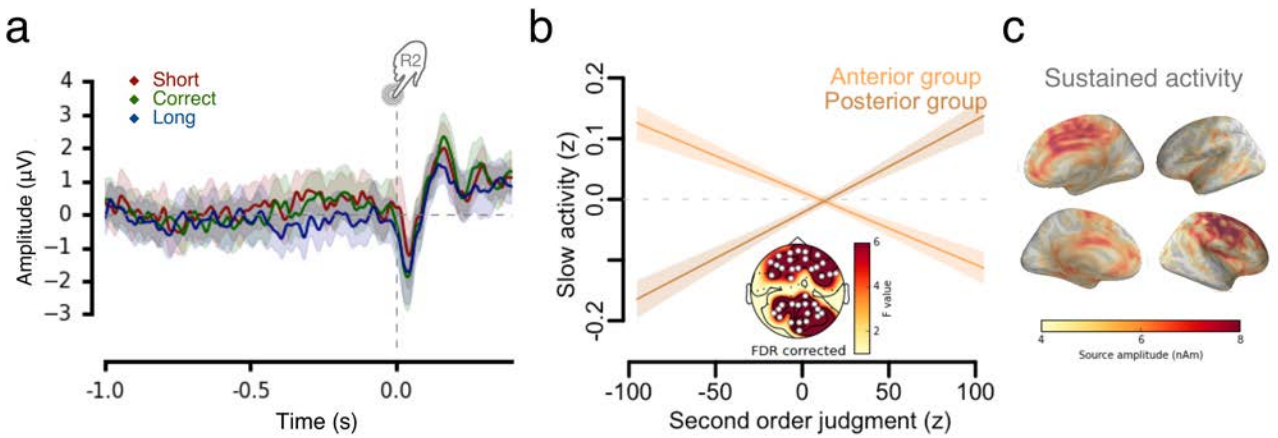

Figure 6. Sustained activity locked to the end of the duration production is indicative of SOJ. (**a**) Time courses and topographical plots of EEG activity 1s prior to the second keypress as a function of SOJ. (**b**) Cortical source estimates collapsed over all conditions. Motor and mid-frontal regions were the most likely origins of the signal. (**c**) GAMM model fit to slow brain activity preceding the second key press (-0.4-0s): the regression plot shows how sustained activity covaried with SOJ. Statistical details in **Supplementary Table 3**, **4**. Topographical maps show significant MEG sensors.

bioRxiv preprint doi: https://doi.org/10.1101/206086; this version posted October 19, 2017. The copyright holder for this preprint (which was not certified by peer review) is the author/funder, who has granted bioRxiv a license to display the preprint in perpetuity. It is made available under aCC-BY-NC-ND 4.0 International license.

Post-interval signatures of temporal error-monitoring

A seminal signature of error monitoring and metacognitive inference is the Error Related Negativity (ERN), which is typically observed after a decisional error has been committed (Yeung et al., 2004; Holroyd & Coles, 2004). As the sources of the ERN are typically located in cingulate cortices, we mainly focused the analysis on EEG data (although contrasts were also ran on MEG), which is more sensitive to midline structures. Surprisingly, contrasting evoked brain responses following the second button press did not elicit significant differences across FOJ or SOJ conditions (**Supplementary Fig. 7;** all $p > 0.1$). The lack of differential ERF/P allowed excluding that refractory effects could play a role at the interval offset (Kononowicz & Van Rijn, 2014).

To fully explore the post-duration evaluation period (0 to 0.4 s following the second button press), we then performed spatiotemporal cluster permutation tests in time-frequency data. We found significant clusters in the alpha band (α, 8-14 Hz) as a function of performance in FOJ (**Fig. 7a**, $p = 0.035$) with main sources originating in the medial and prefrontal regions (**Fig. 7a**, bottom row). Using single-trial GAMM analysis on normalized mean α power revealed a significant group of electrodes showing a linear relationship between α power and FOJ (**Fig. 7b**, **Supplementary Table 5**); another cluster showed a significant linear relationship in the theta band (4-7 Hz) with FOJ (**Supplementary Fig. 8**). A distinct cluster of electrodes revealed a significant cluster of α power inversely correlating with SOJ (**Fig. 7c**, $p = 0.031$) so that trials judged as 'long' were associated with larger α power alpha decreases (**Fig. 7c**). Source analysis revealed bilateral sources in the precuneus (**Fig. 7c**, bottom row), a region markedly different from those which contributed to the FOJ effects. Considering that the sources at the origin of the FOJ and SOJ α power effects were distinct (**Fig. 7ac**), we refitted the GAMM model without including the FOJ term. This analysis revealed a significant group of electrodes for which α power was linearly predicting SOJ (**Fig. 7d**, **Supplementary Table 6**). As for the FOJ fits, the linear relationship between SOJ and post-interval α power indicated that the post-duration production was sensitive to the whole spectrum of SOJ.

The linear trend of α power following FOJ was surprising given that error detection would predict a V-shaped pattern expressed as the typical ERN (Yeung et al., 2004; Holroyd & Coles, 2004): trials considered to be too short or too long were expected to yield a larger magnitude of error signal coding for the difference between the internal duration variable and the behavioral outcome. Instead, we found that α power following FOJ was indicative of the directional difference (or self-assessed residual error) between being too short and being too long.

bioRxiv preprint doi: https://doi.org/10.1101/206086; this version posted October 19, 2017. The copyright holder for this preprint (which was not certified by peer review) is the author/funder, who has granted bioRxiv a license to display the preprint in perpetuity. It is made available under aCC-BY-NC-ND 4.0 International license.

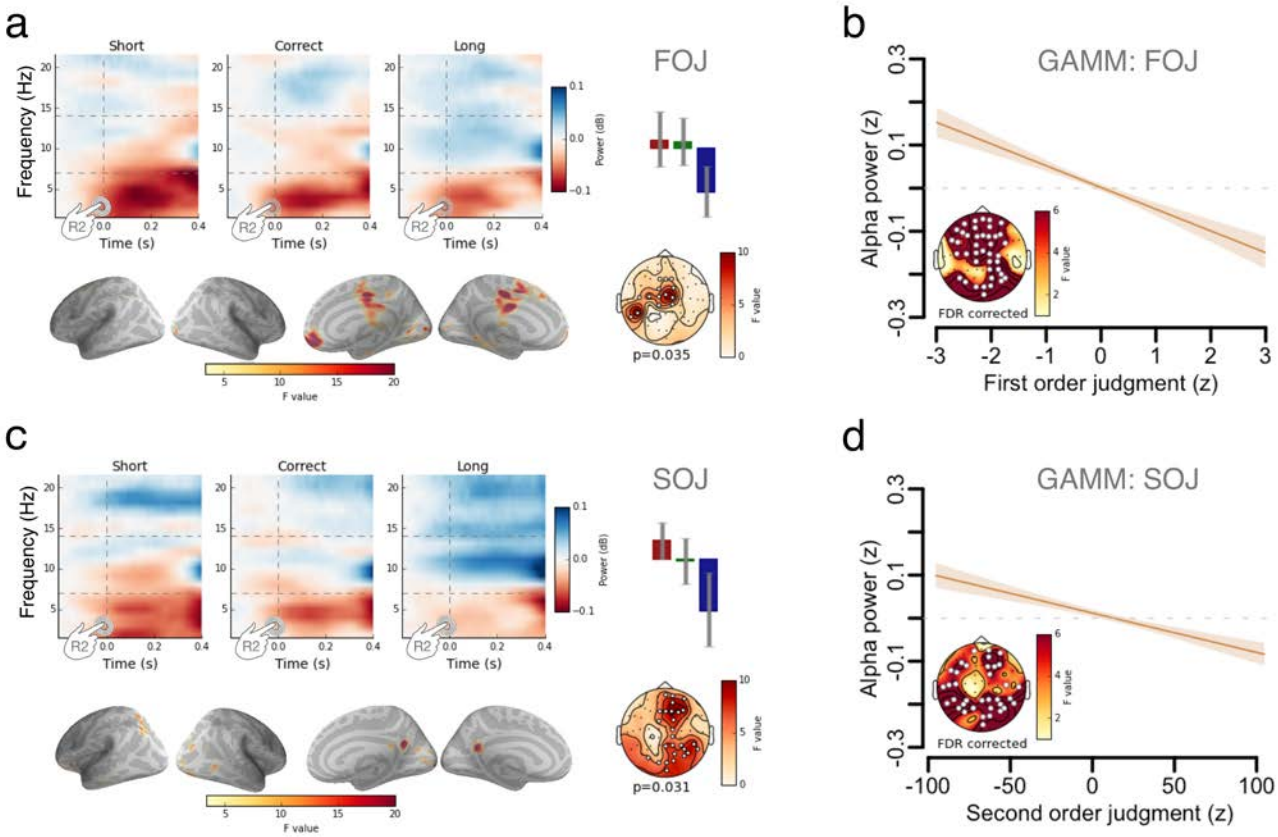

Figure 7. Post-interval signatures of FOJ and SOJ. (**a**) Cluster-based permutation test of EEG α power (8-14 Hz) contrasting the FOJ conditions. Alpha power time courses sorted as a function of FOJ categories found in the most significant electrodes (cluster-based permutation F-tests). The bar plot shows the averaged value in the significant cluster for all three conditions. Source estimates are provided. (**b**) Time-frequency spectrum for the sensor with the largest F value for FOJ based cluster. Source estimates illustrated contrasted α power for FOJ (uncorrected F-map) found in medial central and prefrontal regions. (**c**) The results of GAMM model fits to post-interval alpha power. The topographical maps show the distribution of significant EEG locations. Statistical details in **Supplementary Table 5**. (**d**) Cluster-based permutation test of EEG alpha power (8-14 Hz) contrasting the SOJ conditions. Alpha power time courses sorted as a function of SOJ categories found in the sensor with the highest F-value. Gray area indicates latencies at which β power significantly differed across conditions with cluster-based permutation F-tests. (**e**) Time-frequency spectrum for the sensor with the largest F value for SOJ based cluster. The alpha band is marked by horizontal grey lines. The brain images display the uncorrected F-map contrasting FOJ driven alpha power effect FOJ in the source space. The strongest source originated from the precuneus. (**f**) The results of GAMM model fits where the FOJ term was excluded to post-interval alpha power. The topographical maps show the distribution of significant EEG locations. Statistical details in **Supplementary Table 6**.

DISCUSSION

Using a temporal metacognition task with time-resolved neuroimaging and statistical modeling, we investigated how the human brain monitors its self-generated timing. We report several main findings: first, humans can maintain their precision of temporal production over time despite implicit changes and drifts in mean duration values (FOJ). Second, human participants can accurately self-evaluate the signed error magnitude of their temporal productions (SOJ). Third, the power of β oscillatory activity following the initiation of the time interval was an accurate predictor of FOJ, even more so when participants were aware of their time-errors (SOJ). In particular, we report that the distance in β state-space separating the self-generated

bioRxiv preprint doi: https://doi.org/10.1101/206086; this version posted October 19, 2017. The copyright holder for this preprint (which was not certified by peer review) is the author/funder, who has granted bioRxiv a license to display the preprint in perpetuity. It is made available under aCC-BY-NC-ND 4.0 International license.

time intervals was indicative of the precision with which an individual could infer their performance. Fourth, sustained activity locked to the termination of the generated time interval provided a distinctive signature of second order decision. Fifth, α power following temporal production negatively correlated with both SOJ and FOJ in different medial regions implicated in self-monitoring and metacognition. Altogether, we interpret our results as supporting the availability of an internal state variable coding for duration, which sets up the goal of a state-dependent trajectory for time production. The metacognitive inferences would consist in reading out or decoding the internal state variables, consistent with a recent proposal (Fleming & Daw, 2017) and possibly relying on forward-inverse models of state-dependent computations in motor systems (Harris & Wolpert, 1998). We review and discuss the main evidence supporting this viewpoint along with the limitations of the current study.

β power a marker of state variable coding for time

Our behavioral results build on a recent report (Akdogan & Balci, 2017) by showing that participants can report the signed error magnitude of self-generated time intervals. This observation provides support to the notion that metacognition is a self-referential process (Block, 2005; Fleming & Daw, 2017) in turn questioning which mechanisms may support inference of self-generated dynamics (e.g., Kepecs et al, 2008). Departing from the basic requirements of the volitional task used here, the second button press (timed action) may rely on an internal state variable informing *when* the second button press should be made, given the first button press has occurred. The post-movement rebound of β oscillations has seminally been proposed to reflect the idling state of motor cortices (Pfurtscheller et al., 1996) possibly sensitive to sensory afferents (Casimi et al., 2001). That the power of β oscillations post-movement be stronger (smaller) for timed intervals that were longer (shorter) is parsimoniously consistent with the notion that the strength of network inhibition or idling would be predictive of the produced time interval (FOJ): the stronger the inhibition, the longer the time delay before the next button press can occur.

However, it is important to add a few more observations, so as to not trivialize the importance of β power as passive motor rebound, notably in light of recent studies indicating active cognitive components encoded in the β rebound (Tan et al., 2016). *First*, we found no significant impact of simultaneous EMG in the β effect that was indicative of FOJ, providing no evidence for the implication of the strength or afferent feedback confounded with time estimation. *Second*, the variability in β power did not appear to reflect random variance in time production (or explicit variance induced by the participant, cf. control experiment), but the actual time interval that participants were subsequently aware of. In fact, our results suggested that β power was even more telling of an individual's FOJ when participants correctly self-estimated their FOJ (SOJ). Considering that β power reflects the amount of inhibition in a network (Whittington et al., 2000; Wang, 2010), β power *de facto* provides an estimation of the time delay before the next network update can be made, which, in our context, corresponds to the next movement - consistent with general motor inhibition schemes (Duque et al., 2017). *Additionally*, that the power of β oscillations determines the duration of network inhibition is

bioRxiv preprint doi: https://doi.org/10.1101/206086; this version posted October 19, 2017. The copyright holder for this preprint (which was not certified by peer review) is the author/funder, who has granted bioRxiv a license to display the preprint in perpetuity. It is made available under aCC-BY-NC-ND 4.0 International license.

consistent with the implication of β oscillations in predictive timing (Arnal & Giraud, 2012) and in the notion of an idle state until network updating or reorganization (Engel & Fries, 2010; Spitzer & Haegens, 2017). The power of β has been repeatedly shown to reflect explicit time estimation and prediction (Kononowicz & Van Rijn, 2015, Fujioka et al., 2010) not only in motor timing (Bartolo et al., 2015) but also in sensory-driven duration estimations (Kulashekhar et al., 2015). Hence, we suggest that, because the power of β oscillations is indicative of the strength of inhibition in the network, it also naturally provides a state-dependent variable, which could be used as a duration code.

It is noteworthy that this observation departs away from the notion that time estimation relies on the accumulation of sensory or internal evidence (Buonomano & Maass, 2009; Buhusi & Meck, 2009; Hardy & Buonomano, 2016; Kononowicz & Penney, 2016; van Wassenhove, 2016). As depicted in **Fig. 8**, our state-variable hypothesis rather suggests that, by indicating the amount of inhibition in the network, β power inherently determines the planned trajectory that the network will subsequently follow. Hence, the initial value of β power may be sufficient to predict the time interval that will be produced by participants, and this was essentially captured by the positive interaction between FOJ and β power in our study. Additionally, the initial parameters (mean, noise) defined by this state variable would be predictive of the cascade of neural events leading to the next volitional button press (**Fig. 8**). With respect to behavioral outcome, the second press would be the outcome of a planned trajectory with limited revisions - or vetoing - shortly before the course of the next action, a scenario that has been recently described (Schultze-Kraft et al., 2016). Until reaching the state at which the motor plan for the second button press was initialized, the uncertainty in β state-space would thus reflect the uncertainty with which a decoder or a reader may estimate the duration. This interpretation is consistent with two distinct results: β power was non-linearly related to SOJ with increased β power for trials in which participants provided an accurate metacognitive inference and, second, in the state-space analysis, the more distinct the β state-space trajectories leading to a FOJ category were, the better participants were at self-estimating their time errors. This view thus supports the working hypothesis that network states (Maass et al., 2002; Laje & Buonomano, 2013) or population vectors (Rigotti et al., 2013) may provide a duration code subsequently used for classification by reader units (Maass et al., 2002; Sussillo & Abbott, 2009), serving as self-referential read-out in temporal cognition (van Wassenhove, 2009). Future neurophysiological and neurocomputational work could test the possibility of training such network models.

bioRxiv preprint doi: https://doi.org/10.1101/206086; this version posted October 19, 2017. The copyright holder for this preprint (which was not certified by peer review) is the author/funder, who has granted bioRxiv a license to display the preprint in perpetuity. It is made available under aCC-BY-NC-ND 4.0 International license.

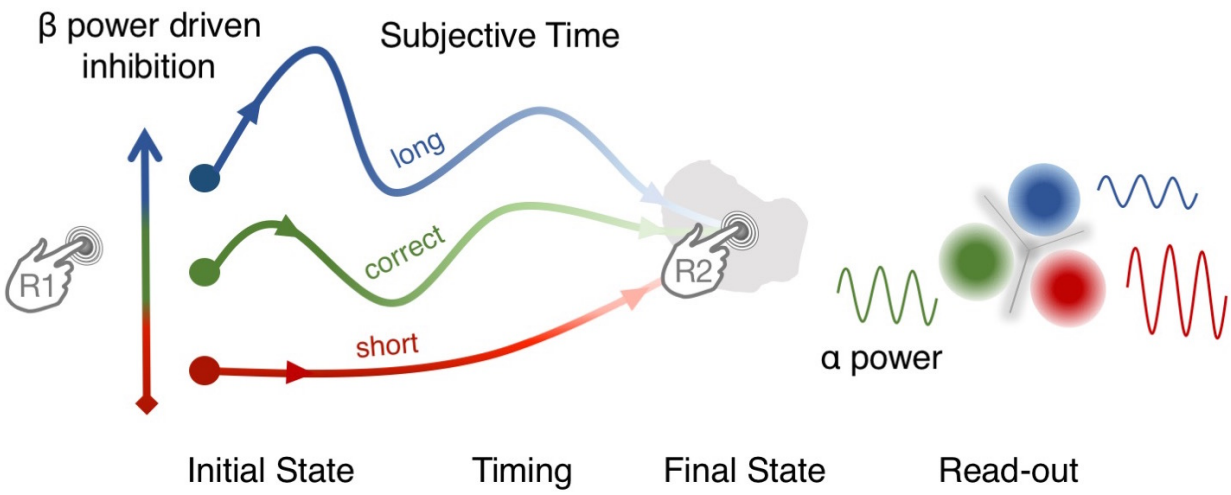

Figure 8. Synthetic view of the role of β oscillations in timing and temporal metacognition. The β power at the onset of the interval determines a network trajectory set by the initial level of inhibition in the network (increasing β power as network inhibition from red to blue). The initial network state and subsequent trajectory determine the motor timing goal. The separation of network trajectories allows to read out (through alpha oscillation) the network state associated with a certain motor timing goal.

Markers of metacognitive inference as internal state variable readout

The non-linear interaction between FOJ and SOJ, and the spread of β state-space trajectories indicative of an individual's metacognitive ability were also used by the second order decision system *before* the end of the trial. The notion that β power may be used to compute second order decision is consistent with theoretical work suggesting that secondary read-out networks can learn to interpret the contingencies in the first order network (Buonomano & Maass, 2009; Cleeremans et al., 2007; Deneve et al., 1999; Dayan & Abbott, 2001; Pouget et al., 1998). In support of this theoretical work, pulvinar neurons have been shown to encode confidence, a second order variable, independently of other areas processing first order variables; this study thus suggested that one population of neurons can read-out neural population that encode primary sensory variables (Komura et al., 2013). Other studies have also suggested that particular brain regions independently code for first and second order signals (Lak et al., 2014). In line with these ideas, the mapping between β power and duration interval may be realized via networking through higher order brain regions. For example, prefrontal cortex, implicated in timing (Kim et al., 2017), monitor signals in motor cortex (Narayanan & Laubach; 2006) and such anatomical separation was found following the termination of the timed interval: larger α power were found for FOJ and SOJ that were shorter than the target duration, whereas smaller α power were found for FOJ and SOJ that were longer than the target duration. α oscillations have been implicated in performance monitoring (van Driel et al., 2012) and the cortical sources observed here were consistent with the acknowledged role of midline cingulate regions in self-monitoring (Miyamoto et al., 2017) and error detection (Ullsperger et al., 2014). The differences in FOJ originated from prefrontal cortices and ACC, whereas differences in SOJ implicated the precuneus, which has been reported during confidence judgments (De Martino et al., 2013), error processing (Menon et al., 2001) and intentional actions, self-awareness and self-processing (Den Ouden et al., 2005). Gray matter volume in precuneus predicts

bioRxiv preprint doi: https://doi.org/10.1101/206086; this version posted October 19, 2017. The copyright holder for this preprint (which was not certified by peer review) is the author/funder, who has granted bioRxiv a license to display the preprint in perpetuity. It is made available under aCC-BY-NC-ND 4.0 International license.

introspective accuracy (Fleming et al., 2010), and metacognitive efficiency in memory (McCurdy et al., 2013). Altogether, this pattern of results following the end of the time interval suggest that signals are integrated in the performance monitoring system (Ullsperger et al., 2014).

Conclusions

We showed that the brain can read-out self-generated signals to assess timing together with time errors. The spread of an individual's β power trajectories during timing was indicative of the individual's metacognitive inference. Our results suggest that network inhibition (β power) instantiates a state variable determining future network trajectory, thus providing a code for duration.

METHODS

Participants

Nineteen right-handed volunteers (11 females, mean age: 24 years old) with no self-reported hearing/vision loss or neurological pathology were recruited for the experiment and received monetary compensation for their participation. Prior to the experiment, each participant provided a written informed consent in accordance with the Declaration of Helsinki (2008) and the Ethics Committee on Human Research at Neurospin (Gif-sur-Yvette). The data of seven participants were excluded from the analysis due to the absence of anatomical MRI, technical issues with the head positioning system during MEG acquisition, abnormal artifacts during MEG recordings, and two participants not finishing the experiment. These datasets were excluded *a priori* and were not visualized or inspected. Hence, the final sample comprised twelve participants (7 females, mean age: 24 y.o.). All but two participants performed six experimental blocks; the first block was removed for one participant due to excessive artifacts, the last block was removed for another participant who did not conform to the requirements of the task.

Stimuli and Procedure

Before the MEG acquisitions, participants were explained they were taking part in a time estimation experiment, and written instructions were provided explaining all steps of the experimental protocol. In a given trial, the participant had to perform three successive steps: first, the participant produced a 1.45 s time interval; second, they self-estimated their time production as too short or too long as compared to the instructed time interval and third, they received feedback on their produced time interval (**Fig. 1a**). We will refer to the produced time interval as the first order temporal judgment (FOJ), and to the self-estimation of the first order judgment as second order temporal judgment (SOJ). The feedback participants received was for all trials in the 1st and in 4th experimental block, or on 15% of the trials in the other blocks (**Fig. 1a**). To tailor an accurate feedback for each individual, a perceptual threshold for duration discrimination of the same 1.45 s duration

bioRxiv preprint doi: https://doi.org/10.1101/206086; this version posted October 19, 2017. The copyright holder for this preprint (which was not certified by peer review) is the author/funder, who has granted bioRxiv a license to display the preprint in perpetuity. It is made available under aCC-BY-NC-ND 4.0 International license.

was collected before the experiment; this individual threshold was used to scale the spacing of the feedback categories as too short, correct or too long (**Fig. 1b**) as well as change the feedback unbeknownst of the participant in blocks 4 to 6.

Each trial started with the presentation of a fixation cross "+"on the screen indicating participants they could start whenever they decided to (**Fig. 1a**). The inter-trial interval ranged between 1 s and 1.5 s. Participants initiated their production of the time interval with a brief but strong button press once they felt relaxed and ready to start. Once they estimated that a 1.45 s interval had elapsed, they terminated the interval by another brief button press. To initiate and terminate their time production (FOJ) participants were asked to press the top button on Fiber Optic Response Pad (FORP, Science Plus Group, DE) using their right thumb (**Fig. 1b**). The "+" was removed from the screen during the estimation of the time interval to avoid any sensory cue or confounding responses in brain activity related to the FOJ. Following the production of the time interval, participants were asked to self-estimate their time estimation (second order judgment; **Fig 1b**). For this, participants were provided with a scale displayed on the screen 0.4 s after the keypress that terminated the produced time interval. Participants could move a cursor continuously using the yellow and green FORP buttons (**Fig. 1b**). Participants were instructed to place the cursor according to how close they thought their FOJ was with respect to the instructed target interval indicated by the sign '~' placed in the middle of the scale. Participants placed the cursor to indicate whether they considered their produced time interval to be too short ('--', left side of the scale) or too long ('++', right side of the scale). Participants were instructed to take as much time as needed to be accurate in their SOJ and there was no time limit imposed on participants.

Following the completion of the SOJ, participants received feedback displayed on a scale identical to the one used for SOJ. The row of five symbols indicated the length of the just produced FOJ (**Fig. 1a).** The feedback range was set to the value of the perceptual threshold estimated on a per (mean population threshold = 0.223 s, SD = 0.111 s). A near correct FOJ yielded the middle '~' symbol to turn green; a too short or too long FOJ turned the symbols '-' or '+' orange, respectively (**Fig. 1b**); a FOJ that exceeded these categories turned the symbols '- -' or '++' red. In Block 1 and 4, feedback was provided in all trials; in Block 2, 3, 5 and 6, feedback was randomly assigned to 15% of the trials (**Fig. 1a**). From Block 4 on, and unbeknownst to participants, the target duration was increased to 1.45 + (*individual threshold*/2; mean population duration = 1.56 s*)*. In Block 1 and 4, participants had to produce 100 trials; in Block 2, 3, 5, and 6, participants produced 118 trials. Between the experimental blocks, participants were reminded to produce the target duration of 1.45 s as accurately as possible and to maximize the number of correct trials in each block.

Estimation of temporal discrimination threshold

The psychoacoustics toolbox was used to calculate the temporal discrimination threshold for each participant (Soranzo & Grassi, 2014) by adapting the available routine "DurationDiscriminationPureTone" provided in the toolbox. An adaptive procedure was chosen using a staircase method with a two-down one-up rule, and stopped after twelve reversals (Levitt, 1971). For each trial, three identical tones of 1 kHz were presented to the participant. One of the tones lasted longer than 1.45 sec (deviant tone) while the other 2 tones lasted

bioRxiv preprint doi: https://doi.org/10.1101/206086; this version posted October 19, 2017. The copyright holder for this preprint (which was not certified by peer review) is the author/funder, who has granted bioRxiv a license to display the preprint in perpetuity. It is made available under aCC-BY-NC-ND 4.0 International license.

precisely 1.45 sec (standard tones). The position of the deviant tone changed randomly across trials. The task was to identify the deviant tone and to give its position in the sequence. Tones were provided by earphones binaurally. The value of the correct category was set as *target duration* +/– (*threshold*/3), the lower and upper limit values were set as *target duration* +/– (2* *individual threshold*/3). These values were used to provide feedback to participants.

Simultaneous M/EEG recordings

The experiment was conducted in a dimly-lit, standard magnetically-shielded room located at Neurospin (CEA/DRF) in Gif-sur-Yvette. Participants sat in an armchair with eyes open looking at a screen used to show visual stimuli using a projector located outside of the magnetically shielded room. Participants were asked to respond by pushing a button on a FORP response pad (Science Plus Group, DE) held in their right hand. Electromagnetic brain activity was recorded using the whole-head Elekta Neuromag Vector View 306 MEG system (Neuromag Elekta LTD, Helsinki) equipped with 102 triple-sensors elements (two orthogonal planar gradiometers, and one magnetometer per sensor location) and the 64 native EEG system using Ag-AgCl electrodes (EasyCap, Germany) with impedances below 15 kΩ. Participants were seated in upright position and their head position was measured before each block using four head-position coils placed over the frontal and the mastoid areas. The four head-position coils and three additional fiducial points (nasion, left and right pre-auricular areas) were used during digitization to help with co-registration of the individual's anatomical MRI. MEG and EEG (M/EEG) recordings were sampled at 1 kHz and band-pass filtered between 0.03 Hz and 330 Hz. The electro-occulograms (EOG, horizontal and vertical eye movements), -cardiograms (ECG), and -myograms (EMG) were recorded simultaneously with MEG. The head position with respect to the MEG sensors was measured using coils attached to the scalp. The locations of the coils and EEG electrodes were digitized with respect to three anatomical landmarks using a 3D digitizer (Polhemus, US/Canada). Stimuli were presented using a PC running Psychtoolbox software (Brainard, 1997) that has been executed in Matlab environment.

Data Analysis

M/EEG data preprocessing

Signal Space Separation (SSS) was applied to decrease the impact of external noise on recorded brain signals (Taulu & Simola, 2006). SSS correction, head movement compensation, and bad channel rejection was done using MaxFilter Software (Elekta Neuromag). Trials containing excessive ocular artifacts, movement artifacts, amplifier saturation, or SQUID artifacts were automatically rejected using rejection criterion applied on magnetometers ($55e^{-12}$ T/m) and on EEG channels ($250e^{-6}$ V). Trial rejection was performed using epochs ranging from - 0.8 s to 2.5 s following the first press initiating the time production trial. Eye blinks, heart-

bioRxiv preprint doi: https://doi.org/10.1101/206086; this version posted October 19, 2017. The copyright holder for this preprint (which was not certified by peer review) is the author/funder, who has granted bioRxiv a license to display the preprint in perpetuity. It is made available under aCC-BY-NC-ND 4.0 International license.

beats, and muscle artifacts were corrected using Independent Component Analysis (Bell & Sejnowski, 1995) with mne-python. Baseline correction was applied using the mean value ranging from -0.3 s to -0.1 s before the first key press.

Preprocessed M/EEG data were then analyzed using MNE Python 0.13 (Gramfort et al., 2014) and custom written Python code. For time-domain evoked response analysis, a low-pass zero phase lag FIR filter (40 Hz) was applied to raw M/EEG data. For time frequency analyses, raw data were filtered using a double-pass bandpass FIR filter (0.8 – 160 Hz). The high-pass cutoff was added to remove slow trends which could lead to instabilities in time frequency analyses. To reduce the dimensionality, all evoked and time-frequency analyses were performed on virtual sensor data combining magnetometers and gradiometers into single MEG sensor types using '*as_type*' method from MNE-Python 0.13 for gradiometers. This procedure largely simplified visualization and statistical analysis without losing information provided by all types of MEG sensors (gradiometers and magnetometers).

M/EEG-aMRI coregistration

Anatomical Magnetic Resonance Imaging (aMRI) was used to provide high-resolution structural images of each individual's brain. The anatomical MRI was recorded using a 3-T Siemens Trio MRI scanner. Parameters of the sequence were: voxel size: 1.0 x 1.0 x 1.1 mm; acquisition time: 466s; repetition time TR = 2300 ms; and echo time TE= 2.98 ms. Volumetric segmentation of participants' anatomical MRI and cortical surface reconstruction was performed with the FreeSurfer software (http://surfer.nmr.mgh.harvard.edu/). A multi-echo FLASH pulse sequence with two flip angles (5 and 30 degrees) was also acquired (Jovicich et al., 2006; Fischl et al., 2004) to improve co-registration between EEG and aMRI. These procedures were used for group analysis with the MNE suite software (Gramfort et al., 2014). The co-registration of the M/EEG data with the individual's structural MRI was carried out by realigning the digitized fiducial points with MRI slices. Using mne_analyze within the MNE suite, digitized fiducial points were aligned manually with the multimodal markers on the automatically extracted scalp of the participant. To insure reliable coregistration, an iterative refinement procedure was used to realign all digitized points with the individual's scalp.

MEG source reconstruction

Individual forward solutions for all source locations located on the cortical sheet were computed using a 3-layers boundary element model (BEM) constrained by the individual's aMRI. Cortical surfaces extracted with FreeSurfer were sub-sampled to 10,242 equally spaced sources on each hemisphere (3.1 mm between sources). The noise covariance matrix for each individual was estimated from the baseline activity of all trials and all conditions. The forward solution, the noise covariance and source covariance matrices were used to calculate the dSPM estimates (Dale et al., 2000). The inverse computation was done using a loose orientation constraint (loose = 0.4, depth = 0.8) on the radial component of the signal. Individuals' current source estimates were registered on the Freesurfer average brain for surface based analysis and visualization.

bioRxiv preprint doi: https://doi.org/10.1101/206086; this version posted October 19, 2017. The copyright holder for this preprint (which was not certified by peer review) is the author/funder, who has granted bioRxiv a license to display the preprint in perpetuity. It is made available under aCC-BY-NC-ND 4.0 International license.

ERF/P analysis

The analyses of evoked-related fields (ERF) and potentials (ERP) with MEG and EEG, respectively, focused on the quantification of the amplitude of slow evoked components using non-parametric cluster-based permutation tests which control for multiple comparisons (Maris & Oostenveld, 2007. This analysis combined all sensors and electrodes into the analysis without predefining a particular subset of electrodes or sensors, allowing to keep the set of MEG and EEG data as similar and consistent as possible. We used a period ranging from 0.3 s to 0.1 s before the first press as a baseline. For the ERF/P analysis the data were low-pass filtered using 40 Hz FIR filter.

Time-frequency analysis

To analyze the oscillatory power in different frequency bands, we used a single Hanning taper with an adaptive time window of 5 cycles per frequency in 4 ms steps for frequencies ranging from 3 to 100 Hz. We used a period ranging from 0.3 s to 0.1 s before the first press as a baseline. The data were processed using '*tfr_morlet'* function from MNE-Python. Statistical analyses were performed on theta (3-7 Hz), alpha (8-14 Hz), β (15-40 Hz), and gamma bands (41-100 Hz) submitted to spatiotemporal cluster permutation tests in the same way as for evoked response analyses. Both time-frequency and power spectral density (PSD) estimates were computed using discrete spheroidal sequences tapers (Slepian, 1978). PSD estimates were computed in 1 Hz steps.

Cluster based statistical analysis of MEG and EEG data

Cluster-based analyses identified significant clusters of neighboring electrodes or sensors in the millisecond time dimension. To assess the differences between the experimental conditions as defined by behavioral outcomes, we ran cluster-based permutation analysis (Maris & Oostenveld, 2007), as implemented by MNE-Python by drawing 1000 samples for the Monte Carlo approximation and using FieldTrip's default neighbor templates. The randomization method identified the MEG virtual sensors and the EEG electrodes whose statistics exceeded a critical value. Neighboring sensors exceeding the critical value were considered as belonging to a significant cluster. The cluster level statistic was defined as the sum of values of a given statistical test in a given cluster, and was compared to a null distribution created by randomizing the data between conditions across multiple participants. The p-value was estimated based on the proportion of the randomizations exceeding the observed maximum cluster-level test statistic. Only clusters with corrected p-value < 0.05 are reported. For visualization, we have chosen to plot the MEG sensor or the EEG electrode of the significant cluster, with the highest statistical power.

Behavioral data analysis

bioRxiv preprint doi: https://doi.org/10.1101/206086; this version posted October 19, 2017. The copyright holder for this preprint (which was not certified by peer review) is the author/funder, who has granted bioRxiv a license to display the preprint in perpetuity. It is made available under aCC-BY-NC-ND 4.0 International license.

The analysis of behavioral data was performed as in the GAMMs framework as fully described below in the *Single-trial analysis of MEG and EEG data*, unless stated otherwise in the Results section. Each model was fitted with subject as a random factor. For the Block analysis, Block was included as a fixed factor. For the analysis of metacognitive inference, SOJ was entered as a linear predictor of FOJ. Relative model comparison was performed using Akaike Information Criterion (AIC) and χ^2 test.

Binning procedure of behavioral and neuroimaging data

All cluster-based analyses were performed on three experimentally-driven conditions defined on the basis of either the objective performance in time production (FOJ: short, correct, long) or the subjective self-estimation (SOJ: short, correct, long) separately for each experimental block. Computing these three conditions within a block focused the analysis on local variations of brain activity as a function of objective or subjective performance. Additionally, to overcome limitations of arbitrary binning, and to capitalize on the continuous performance naturally provided by the time production and time self-estimation tasks, we also used a single trial approach, which allowed the investigation of interactions between the first and second order terms.

Single-trial analysis of MEG and EEG data

To analyze single trial data we used generalized additive mixed models (Wood, 2017; GAMM). Detailed discussions on the GAMM method can be found in elsewhere (Wood, 2017). Here, we briefly introduce the main advantages and overall approach of the method. GAMMs are an extension of the generalized linear regression model in which non-linear terms can be modeled jointly. They are more flexible than simple linear regression models as they do not require that a non-linear function be specified and the specific shape of the non-linear function (i.e. smooth) is determined automatically. Specifically, the non-linearities are modeled by so-called basis functions that consist of several low-level functions (linear, quadratic, etc.). We have chosen GAMMs as they can estimate the relationship between multiple predictors and the dependent variable using a non-linear smooth function. The appropriate degrees of freedom and overfitting concerns are addressed through cross-validation procedures. Importantly, interactions between two nonlinear predictors can be modeled as well. In that case, the fitted function takes a form of a plane consisting of two predictors. Mathematically, this is accomplished by modeling tensor product smooths. Here, we used thin plate regression splines as it seemed most appropriate for large data sets and flexible fitting (Wood, 2003). In all presented analyses, we used a maximum likelihood method for smooth parameter optimization (Wood, 2011). GAMM analyses were performed using the *mgcv* R package (Wood, 2009, version 1.8.12). GAMM results were plotted using the *itsadug* R package (Van Rij et al., 2016, version 1.0.1).

Although not widely used, GAMMs have been proven useful for modeling EEG data (Tremblay & Newman, 2015). Contrary to some of the previous studies using GAMMs for modeling of multidimensional electrophysiological data, sensors were not included as fixed effects. Rather, we took a more conservative approach and fitted the same model for every sensor separately. The resulting p-values were then corrected for

bioRxiv preprint doi: https://doi.org/10.1101/206086; this version posted October 19, 2017. The copyright holder for this preprint (which was not certified by peer review) is the author/funder, who has granted bioRxiv a license to display the preprint in perpetuity. It is made available under aCC-BY-NC-ND 4.0 International license.

multiple comparisons using false discovery rate (FDR) correction (Genovese et al., 2002). For plotting purposes, we collapsed the data across significant sensors after FDR correction and refitted the model.

We fitted the same GAMMs for several neurophysiological measurements chosen on the basis of previous literature. The fitted model contained random effects term for participant and fixed effects that were based on theoretical predictions. Specifically the full model had the following specification: *uV/Tesla/power* ~ s(*FOJ*) + s(*SOJ*) + s(*Incongruence*) + ti(*FOJ, SOJ*) + ti(*FOJ, Incongruence*) + s(*participant,* bs='re'). Besides the random term for participants, the model contained smooth terms for the first and second order judgments, *Incongruence* between the first and second order judgment, and the interaction term between *FOJ* and *Incongruence*. Notably, FOJ, SOJ and other predictors were entered as continuous variables in GAM analyses as opposed to post-hoc experimental conditions which suffered limitations from choosing arbitrary split point in the data.

Although GAMMs have built-in regularization procedures (meaning that they are somewhat inherently resistant against multicollinearity), multicollinearity can been assessed using variance inflation factor (VIF; *fmsb* R package, version 0.5.2). Here, VIF were assessed for the final model and consisted in averaging data from multiple sensors collapsed over a particular variable at hand. None of the VIF values exceeded 1.1, indicating that multicollinearity was unlikely to have had a major influence on the reported findings. Note that Rogerson (2001) recommended maximum VIF value of 5 and the author of *fmsb* recommended value of 10.

Before entering empirical variables in the model, we calculated normalized values or z-scores: trials in which a given variable deviated more than 3 z-scores were removed from further analysis. This normalization was computed separately for every MEG sensor and every EEG electrode. For single-trial analyses of β power in FOJ, we focused on the maximum power within the 0.4 s to 0.8 s period following the first button press. This time window overlapped with the selected time window that was used in cluster analyses. The main difference for the width of the time window is that we used one value for the GAMM and hence insured we capture only the β power elicited by the first button press and not spurious preparatory brain responses to the second button press. For the single-trial analyses of other brain signatures – e.g., sustained evoked activity or alpha oscillations - we focused on the mean values in a given time window.

Demixed Principal Component Analysis (dPCA)

To extract patterns in different frequency bands of averaged brain activity over experimental conditions, we used dPCA analysis (Kobak et al., 2016). Although, dPCA is commonly used in the population analysis of single cell recordings we apply it to collection of sensors, something that is analogical to population of neurons with mixed selectivities. Detailed discussions and proofs of the dPCA method can be found elsewhere (Kobak et al., 2016). In brief, dPCA aims to find a decomposition of the data into latent components that are easily interpretable with experimental conditions, preserving the original data to a maximal extent. The method compresses the data but also demixes dependencies on measured quantity of the task parameters. dPCA is essentially driven by a trade-off between demixing and compression, thus is a mixture of ordinary

bioRxiv preprint doi: https://doi.org/10.1101/206086; this version posted October 19, 2017. The copyright holder for this preprint (which was not certified by peer review) is the author/funder, who has granted bioRxiv a license to display the preprint in perpetuity. It is made available under aCC-BY-NC-ND 4.0 International license.

PCA and linear discriminant analysis (LDA): PCA aims at determining a projection of the data that optimally separates conditions and LDA aims at determining a projection of the data which minimizes the reconstruction error between the projections and the original data. All analyses were performed using a *Python* version of the *dPCA* module (https://github.com/machenslab/dPCA). To prevent overfitting, we used a regularization procedure to find the optimal λ parameter for our dataset, and used a 10-fold cross-validation. We focused dPCA analyses on the two first components (dPCA 1 and dPCA 2) of the βoscillatory activity because they explained on average 73% (SD= 20%) and 26% (SD= 20%) of the overall variance, respectively. Multidimensional distance was quantified as Euclidean distance for both dPCA analysis and for per-sensor analysis.

Robust regression of MEG and EEG data

Robust regression is an alternative to least squares regression when data have outliers or influential observations. It is also an alternative to Spearman's correlation when a more complex model has to be built. Model comparisons were performed using robust F test. All analyses were performed using *robust* R package (Wang et al., 2017, version 0.4-18).

References:

Akdogan, B., & Balci, F. (2017). Are you early or late?: Temporal error monitoring. Journal of Experimental Psychology: General, 146(3), 347-361.

Arnal, L. H., & Giraud, A. -L. (2012). Cortical oscillations and sensory predictions. Trends in Cognitive Sciences, 16(7), 390-398.

Allman, M. J., Teki, S., Griffiths, T. D., & Meck, W. H. (2014). Properties of the internal clock: First-and second-order principles of subjective time. Annual Review of Psychology, 65, 743-771.

Bartolo, R., Prado, L., & Merchant, H. (2014). Information processing in the primate basal ganglia during sensory-guided and internally driven rhythmic tapping. The Journal of Neuroscience, 34(11), 3910-3923.

Bell, A. J., & Sejnowski, T. J. (1995). An information-maximization approach to blind separation and blind deconvolution. Neural Computation, 7(6), 1129-1159.

Block, N. (1995). On a confusion about a function of consciousness. Behavioral and brain sciences, 18(2), 227-247.

Bogacz, R., Brown, E., Moehlis, J., Holmes, P., & Cohen, J. D. (2006). The physics of optimal decision making: A formal analysis of models of performance in two-alternative forced-choice tasks. Psychological Review, 113(4), 700.

Brainard, D. H. (1997). The psychophysics toolbox. Spatial Vision, 10, 433-436.

Bueno, F. D., Morita, V. C., de Camargo, R. Y., Reyes, M. B., Caetano, M. S., & Cravo, A. M. (2017). Dynamic representation of time in brain states. Scientific Reports, 7.

Buhusi, C. V., & Meck, W. H. (2005). What makes us tick? Functional and neural mechanisms of interval timing. Nat Rev Neurosci, 6(10), 755-65.

Buonomano, D. V., & Maass, W. (2009). State-dependent computations: Spatiotemporal processing in cortical networks. Nat Rev Neurosci, 10(2), 113-25.

bioRxiv preprint doi: https://doi.org/10.1101/206086; this version posted October 19, 2017. The copyright holder for this preprint (which was not certified by peer review) is the author/funder, who has granted bioRxiv a license to display the preprint in perpetuity. It is made available under aCC-BY-NC-ND 4.0 International license.

Cassim, F., Szurhaj, W., Sediri, H., Devos, D., Bourriez, J., Poirot, I., . . . Guieu, J. (2000). Brief and sustained movements: Differences in event-related (de)synchronization (ERD/ERS) patterns. Clinical Neurophysiology, 111(11), 2032-2039.

Cleeremans, A., Timmermans, B., & Pasquali, A. (2007). Consciousness and metarepresentation: A computational sketch. Neural Networks, 20(9), 1032-1039.

Dale, A. M., Liu, A. K., Fischl, B. R., Buckner, R. L., Belliveau, J. W., Lewine, J. D., & Halgren, E. (2000). Dynamic statistical parametric mapping: Combining fmri and MEG for high-resolution imaging of cortical activity. Neuron, 26(1), 55-67.

Dayan, P., & Abbott, L. F. (2001). Theoretical neuroscience (Vol. 806). Cambridge, MA: MIT Press.

Deneve, S., Latham, P. E., & Pouget, A. (1999). Reading population codes: A neural implementation of ideal observers. Nature Neuroscience, 2(8), 740-745.

Den Ouden, H. E., Frith, U., Frith, C., & Blakemore, S. -J. (2005). Thinking about intentions. Neuroimage, 28(4), 787-796.

De Martino, B., Fleming, S. M., Garrett, N., & Dolan, R. J. (2013). Confidence in value-based choice. Nature Neuroscience, 16(1), 105-110.

Duque, J., Greenhouse, I., Labruna, L., & Ivry, R. B. (2017). Physiological markers of motor inhibition during human behavior. Trends in Neurosciences, 40(4), 219-236.

Engel, A. K., & Fries, P. (2010). Beta-band oscillations signalling the status quo? Current Opinion in Neurobiology, 20(2), 156-165.

Fleming, S. M., & Dolan, R. J. (2012). The neural basis of metacognitive ability. Phil. Trans. R. Soc. B, 367(1594), 1338-1349.

Fleming, S. M., Dolan, R. J., & Frith, C. D. (2012). Metacognition: Computation, biology and function. Phil. Trans. R. Soc. B, 367(1594), 1280-1286.

Fleming, S. M., & Daw, N. D. (2017). Self-evaluation of decision-making: A general bayesian framework for metacognitive computation. Psychological Review, 124(1), 91-114.

Fleming, S. M., Weil, R. S., Nagy, Z., Dolan, R. J., & Rees, G. (2010). Relating introspective accuracy to individual differences in brain structure. Science, 329(5998), 1541-1543.

Fischl, B., Salat, D. H., van der Kouwe, A. J., Makris, N., Ségonne, F., Quinn, B. T., & Dale, A. M. (2004). Sequence-independent segmentation of magnetic resonance images. Neuroimage, 23, 69-84.

Fujioka, T., Zendel, B. R., & Ross, B. (2010). Endogenous neuromagnetic activity for mental hierarchy of timing. The Journal of Neuroscience, 30(9), 3458-3466.

Genovese, C. R., Lazar, N. A., & Nichols, T. (2002). Thresholding of statistical maps in functional neuroimaging using the false discovery rate. Neuroimage, 15(4), 870-878.

Gold, J. I., & Shadlen, M. N. (2007). The neural basis of decision making. Annu. Rev. Neurosci., 30, 535-574.

Gramfort, A., Luessi, M., Larson, E., Engemann, D.A., Strohmeier, D., Brodbeck, C., Parkkonen, L., Hämäläinen, M.S., (2014). MNE software for processing MEG and EEG data. NeuroImage 86, 446–460.

Gu, B. -M., van Rijn, H., & Meck, W. H. (2015). Oscillatory multiplexing of neural population codes for interval timing and working memory. Neuroscience & Biobehavioral Reviews, 48, 160-185.

Hardy, N. F., & Buonomano, D. V. (2016). Neurocomputational models of interval and pattern timing. Current Opinion in Behavioral Sciences, 8, 250-257.

Harris, C. M., & Wolpert, D. M. (1998). Signal-dependent noise determines motor planning. Nature, 394(6695), 780-784.

Holroyd, C. B., & Coles, M. G. (2002). The neural basis of human error processing: Reinforcement learning, dopamine, and the error-related negativity. Psychological Review, 109(4), 679.

Jovicich, J., Czanner, S., Greve, D., Haley, E., van der Kouwe, A., Gollub, R., . . . MacFall, J. (2006). Reliability in multi-site structural MRI studies: Effects of gradient non-linearity correction on phantom and human data. Neuroimage, 30(2), 436-443.

Kepecs, A., Uchida, N., Zariwala, H. A., & Mainen, Z. F. (2008). Neural correlates, computation and behavioural impact of decision confidence. Nature, 455(7210), 227-231.+

bioRxiv preprint doi: https://doi.org/10.1101/206086; this version posted October 19, 2017. The copyright holder for this preprint (which was not certified by peer review) is the author/funder, who has granted bioRxiv a license to display the preprint in perpetuity. It is made available under aCC-BY-NC-ND 4.0 International license.

Kim, Y., Han, S., Alberico, S. L., Ruggiero, R. N., De Corte, B., Chen, K., & Narayanan, N. S. (2017). Optogenetic stimulation of frontal D1 neurons compensates for impaired temporal control of action in dopamine-depleted mice. Current Biology, 27(1), 39-47.

Kobak, D., Brendel, W., Constantinidis, C., Feierstein, C. E., Kepecs, A., Mainen, Z. F., . . . Machens, C. K. (2016). Demixed principal component analysis of neural population data. ELife, 5, e10989.

Komura, Y., Nikkuni, A., Hirashima, N., Uetake, T., & Miyamoto, A. (2013). Responses of pulvinar neurons reflect a subject's confidence in visual categorization. Nature Neuroscience, 16(6), 749-755.

Kononowicz, T. W., & van Rijn, H. (2015). Single trial βoscillations index time estimation. Neuropsychologia, 75, 381-389.

Kononowicz, T. W., & Van Rijn, H. (2011). Slow potentials in time estimation: The role of temporal accumulation and habituation. Frontiers in Integrative Neuroscience, 5(48).

Kononowicz, T. W., & Penney, T. B. (2016). The contingent negative variation (CNV): Timing isn't everything. Current Opinion in Behavioral Sciences, 8, 231-237.

Kononowicz, T. W., & van Rijn, H. (2014). Decoupling interval timing and climbing neural activity: A dissociation between CNV and N1P2 amplitudes. The Journal of Neuroscience, 34(8), 2931-2939.

Kulashekhar, S., Pekkola, J., Palva, J. M., & Palva, S. (2016). The role of cortical beta oscillations in time estimation. Human Brain Mapping, 37(9), 3262-3281.

Laje, R., & Buonomano, D. V. (2013). Robust timing and motor patterns by taming chaos in recurrent neural networks. Nature Neuroscience, 16(7), 925-933.

Lak, A., Costa, G. M., Romberg, E., Koulakov, A. A., Mainen, Z. F., & Kepecs, A. (2014). Orbitofrontal cortex is required for optimal waiting based on decision confidence. Neuron, 84(1), 190-201.

Lau, H. C., Rogers, R. D., Haggard, P., & Passingham, R. E. (2004). Attention to intention. Science, 303(5661), 1208.

Levitt, H. C. C. H. (1971). Transformed up-down methods in psychoacoustics. The Journal of the Acoustical society of America, 49(2B), 467-477.

Macar, F., & Vidal, F. (2009). Timing processes: An outline of behavioural and neural indices not systematically considered in timing models. Can J Exp Psychol, 63(3), 227-39.

Machens, C. K. (2010). Demixing population activity in higher cortical areas. Frontiers in Computational Neuroscience, 4.

Maass, W., Natschlager, T., Markam, H. (2002). Real-time computing without stable states: A new framework for neural computation based on perturbations. Neural Computation, 14, 2531-2560.

Maris, E., & Oostenveld, R. (2007). Nonparametric statistical testing of eeg-and meg-data. Journal of Neuroscience Methods, 164(1), 177-190.

McCurdy, L. Y., Maniscalco, B., Metcalfe, J., Liu, K. Y., de Lange, F. P., & Lau, H. (2013). Anatomical coupling between distinct metacognitive systems for memory and visual perception. Journal of Neuroscience, 33(5), 1897-1906.

Meck, W. H., Komeily-Zadeh, F. N., & Church, R. M. (1984). Two-step acquisition: Modification of an internal clock's criterion. Journal of Experimental Psychology: Animal Behavior Processes, 10(3), 297.

Meck, W. H. (1988). Hippocampal function is required for feedback control of an internal clock's criterion. Behavioral Neuroscience, 102(1), 54.

Meijer, D., Te, E. W., & Praamstra, P. (2016). Timing of beta oscillatory synchronization and temporal prediction of upcoming stimuli. NeuroImage, 138, 233-241.

Menon, V., Adleman, N. E., White, C. D., Glover, G. H., & Reiss, A. L. (2001). Error-related brain activation during a go/nogo response inhibition task. Human Brain Mapping, 12(3), 131-143.

Merchant, H., Harrington, D. L., & Meck, W. H. (2013). Neural basis of the perception and estimation of time. Annual Review of Neuroscience, 36(0), 313-336.

Miall, R. C., & Wolpert, D. M. (1996). Forward models for physiological motor control. Neural Networks, 9(8), 1265-1279.

Miltner, W. H. R., Braun, C. H., & Coles, M. G. H. (1997). Event-related brain potentials following incorrect feedback in a time-estimation task: Evidence for a generic neural system for error detection. Journal of

bioRxiv preprint doi: https://doi.org/10.1101/206086; this version posted October 19, 2017. The copyright holder for this preprint (which was not certified by peer review) is the author/funder, who has granted bioRxiv a license to display the preprint in perpetuity. It is made available under aCC-BY-NC-ND 4.0 International license.

Cognitive Neuroscience, 9(6), 788-798.

Miyamoto, K., Osada, T., Setsuie, R., Takeda, M., Tamura, K., Adachi, Y., & Miyashita, Y. (2017). Causal neural network of metamemory for retrospection in primates. Science, 355(6321), 188-193.

Narayanan, N. S., & Laubach, M. (2006). Top-down control of motor cortex ensembles by dorsomedial prefrontal cortex. Neuron, 52(5), 921-931.

O'Connell, R. G., Dockree, P. M., Robertson, I. H., Bellgrove, M. A., Foxe, J. J., & Kelly, S. P. (2009). Uncovering the neural signature of lapsing attention: Electrophysiological signals predict errors up to 20 s before they occur. Journal of Neuroscience, 29(26), 8604-8611.

Pfurtscheller, G., Stancák, A., & Neuper, C. (1996). Event-related synchronization (ERS) in the alpha band--an electrophysiological correlate of cortical idling: A review. International Journal of Psychophysiology, 24(1-2), 39-46.

Pouget, A., Zhang, K., Deneve, S., & Latham, P. E. (1998). Statistically efficient estimation using population coding. Neural Computation, 10(2), 373-401.

Rogerson, P. (2001). Statistical methods for geography. Sage.

Rigotti, M., Barak, O., Warden, M. R., Wang, X. J., Daw, N. D., Miller, E. K., & Fusi, S. (2013). The importance of mixed selectivity in complex cognitive tasks. Nature, 497(7451), 585-90.

Schultze-Kraft, M., Birman, D., Rusconi, M., Allefeld, C., Görgen, K., Dähne, S., . . . Haynes, J. -D. (2016). The point of no return in vetoing self-initiated movements. Proceedings of the National Academy of Sciences, 113(4), 1080-1085.

Slepian, D. (1978). Prolate spheroidal wave functions, fourier analysis, and uncertainty: The discrete case. Bell System Technical Journal, 57(5), 1371-1430.

Soranzo, A., & Grassi, M. (2014). PSYCHOACOUSTICS: a comprehensive MATLAB toolbox for auditory testing. Frontiers in psychology, 5, 712.

Sussillo, D., & Abbott, L. F. (2009). Generating coherent patterns of activity from chaotic neural networks. Neuron, 63(4), 544-557.

Spitzer, B., & Haegens, S. (2017). Beyond the status quo: A role for beta oscillations in endogenous content (re-) activation. ENeuro, ENEURO-0170.

Tan, H., Wade, C., & Brown, P. (2016). Post-movement beta activity in sensorimotor cortex indexes confidence in the estimations from internal models. Journal of Neuroscience, 36(5), 1516-1528.

Taulu, S., & Simola, J. (2006). Spatiotemporal signal space separation method for rejecting nearby interference in MEG measurements. Physics in Medicine and Biology, 51(7), 1759-1769.

Tremblay, A., & Newman, A. J. (2015). Modeling nonlinear relationships in ERP data using mixed-effects regression with R examples. Psychophysiology, 52(1), 124-139.

Tzagarakis, C., Ince, N. F., Leuthold, A. C., & Pellizzer, G. (2010). Beta-band activity during motor planning reflects response uncertainty. J Neurosci, 30(34), 11270-7.

Ullsperger, M., Fischer, A. G., Nigbur, R., & Endrass, T. (2014). Neural mechanisms and temporal dynamics of performance monitoring. Trends in Cognitive Sciences, 18(5), 259-267.

Van Rij, J., Wieling, M., Baayen, R.H., van Rijn, H. (2016) Package 'itsadug'. Retrieved on June 13, 2017, from http://cran.r-project.org/web/packages/ itsadug /itsadug.pdf

van Driel, J., Ridderinkhof, K. R., & Cohen, M. X. (2012). Not all errors are alike: Theta and alpha EEG dynamics relate to differences in error-processing dynamics. The Journal of Neuroscience, 32(47), 16795-16806.

Van Rijn, H., Kononowicz, T. W., Meck, W. H., Ng, K. K., & Penney, T. B. (2011). Contingent negative variation and its relation to time estimation: A theoretical evaluation. Frontiers in Integrative Neuroscience, 5.

van Wassenhove, V. (2009). Minding time in an amodal representational space. Philosophical Transactions of the Royal Society B: Biological Sciences, 364(1525), 1815-1830.

van Wassenhove, V. (2016). Temporal cognition and neural oscillations. Current Opinion in Behavioral Sciences, 8, 124-130.

Wang, X. -J. (2010). Neurophysiological and computational principles of cortical rhythms in cognition.

bioRxiv preprint doi: https://doi.org/10.1101/206086; this version posted October 19, 2017. The copyright holder for this preprint (which was not certified by peer review) is the author/funder, who has granted bioRxiv a license to display the preprint in perpetuity. It is made available under aCC-BY-NC-ND 4.0 International license.

Physiological Reviews, 90(3), 1195-1268.

Wang, J., Zamar, R., Marazzi, A., Yohai, V., Salibian-Barrera, M., Maronna, K., Zivot, E., Rocke, D., Martin, D., Maechler, M., Konis K. (2017). Package 'robust'. Retrieved on August 1, 2017, from https://CRAN.R-project.org/package=robust

Wagenmakers, E. -J., & Farrell, S. (2004). AIC model selection using akaike weights. Psychonomic Bulletin & Review, 11(1), 192-196.

Whittington, M. A., Traub, R. D., Kopell, N., Ermentrout, B., & Buhl, E. H. (2000). Inhibition-based rhythms: Experimental and mathematical observations on network dynamics. International Journal of Psychophysiology, 38(3), 315-336.

Wood, S. (2017). Generalized additive models: An introduction with R. CRC press.

Wood, S. N. (2003). Thin plate regression splines. Journal of the Royal Statistical Society: Series B (Statistical Methodology), 65(1), 95-114.

Wood, S. N. (2011). Fast stable restricted maximum likelihood and marginal likelihood estimation of semiparametric generalized linear models. Journal of the Royal Statistical Society: Series B (Statistical Methodology), 73(1), 3-36.

Wood, S. (2009). Package 'mgcv'. Retrieved on February 8, 2017, from http://cran.r-project.org/web/packages/mgcv/mgcv.pdf

Wiener, M., Turkeltaub, P., & Coslett, H. B. (2010). The image of time: A voxel-wise meta-analysis. Neuroimage, 49(2), 1728-40.

Yeung, N., Botvinick, M. M., & Cohen, J. D. (2004). The neural basis of error detection: Conflict monitoring and the error-related negativity. Psychological Review, 111(4), 931-959.

bioRxiv preprint doi: https://doi.org/10.1101/206086; this version posted October 19, 2017. The copyright holder for this preprint (which was not certified by peer review) is the author/funder, who has granted bioRxiv a license to display the preprint in perpetuity. It is made available under aCC-BY-NC-ND 4.0 International license.

SUPPLEMENTARY FIGURES

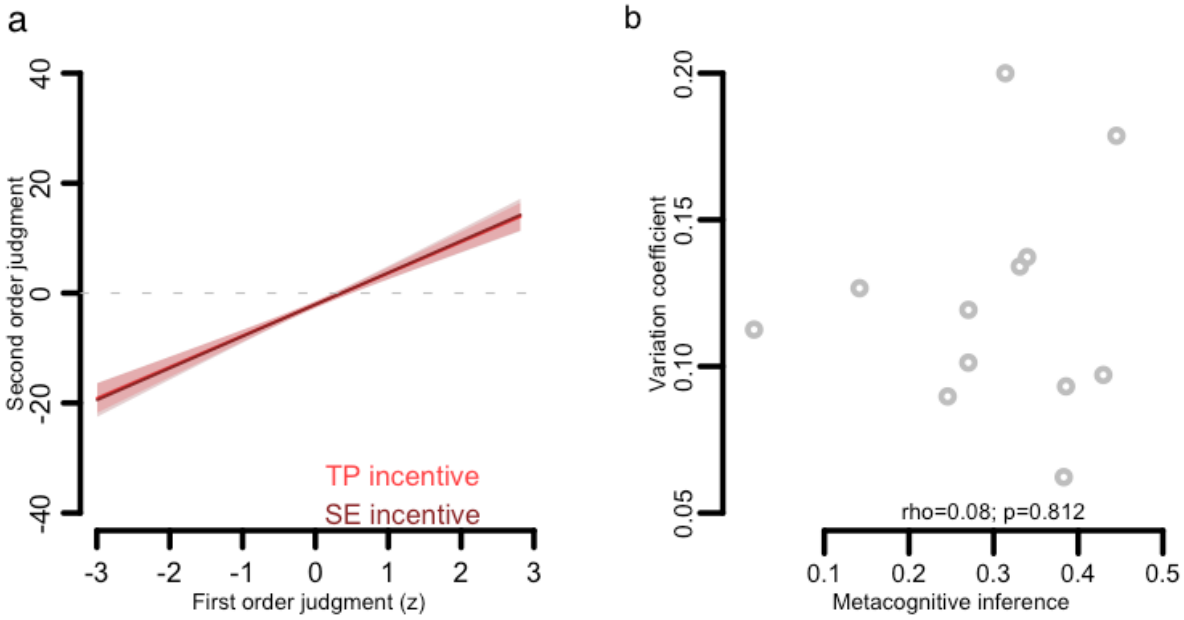

Supplementary Figure 1. Participants solely rely on temporal representation for their SOJ. (**a**) Participants do not modulate their responses based on changes of incentives. The plot depicts behavioral data in the control psychophysical experiment and illustrates the strong link between FOJ and SOJ. Regression lines depict the model fit between the observed SOJ and FOJ estimates for a block with incentive for FOJ (dark red) and another block with an incentive on congruence between FOJ and SOJ (light red). We find no evidence supporting the hypothesis that incentive manipulation would have an impact on SOJ, suggesting that participants in the main task did not use any strategies when performing SOJ.

In the incentive for FOJ block participants received 2 points for a "green" feedback and 1 point for an "orange" feedback. In the incentive for SOJ accuracy block, the distance between FOJ and SOJ category was computed. Participants were given points on each trial according to this distance: the SOJ category boundaries were arbitrary set to -60, -30, +30, and +60 points on the self-evaluation scale. Specifically, when FOJ and SOJ landed in the same category participants received 2 points; they received 1 point when they landed in adjacent categories; and 0 points when categories were different. Nine participants took part in the experiment with two block of 100 trials. (**b**) The spread of FOJ was not related to metacognitive inference. The plot illustrates coefficient of variation over FOJ plotted against metacognitive inference quantified as Spearman's correlation between FOJ and SOJ.

bioRxiv preprint doi: https://doi.org/10.1101/206086; this version posted October 19, 2017. The copyright holder for this preprint (which was not certified by peer review) is the author/funder, who has granted bioRxiv a license to display the preprint in perpetuity. It is made available under aCC-BY-NC-ND 4.0 International license.

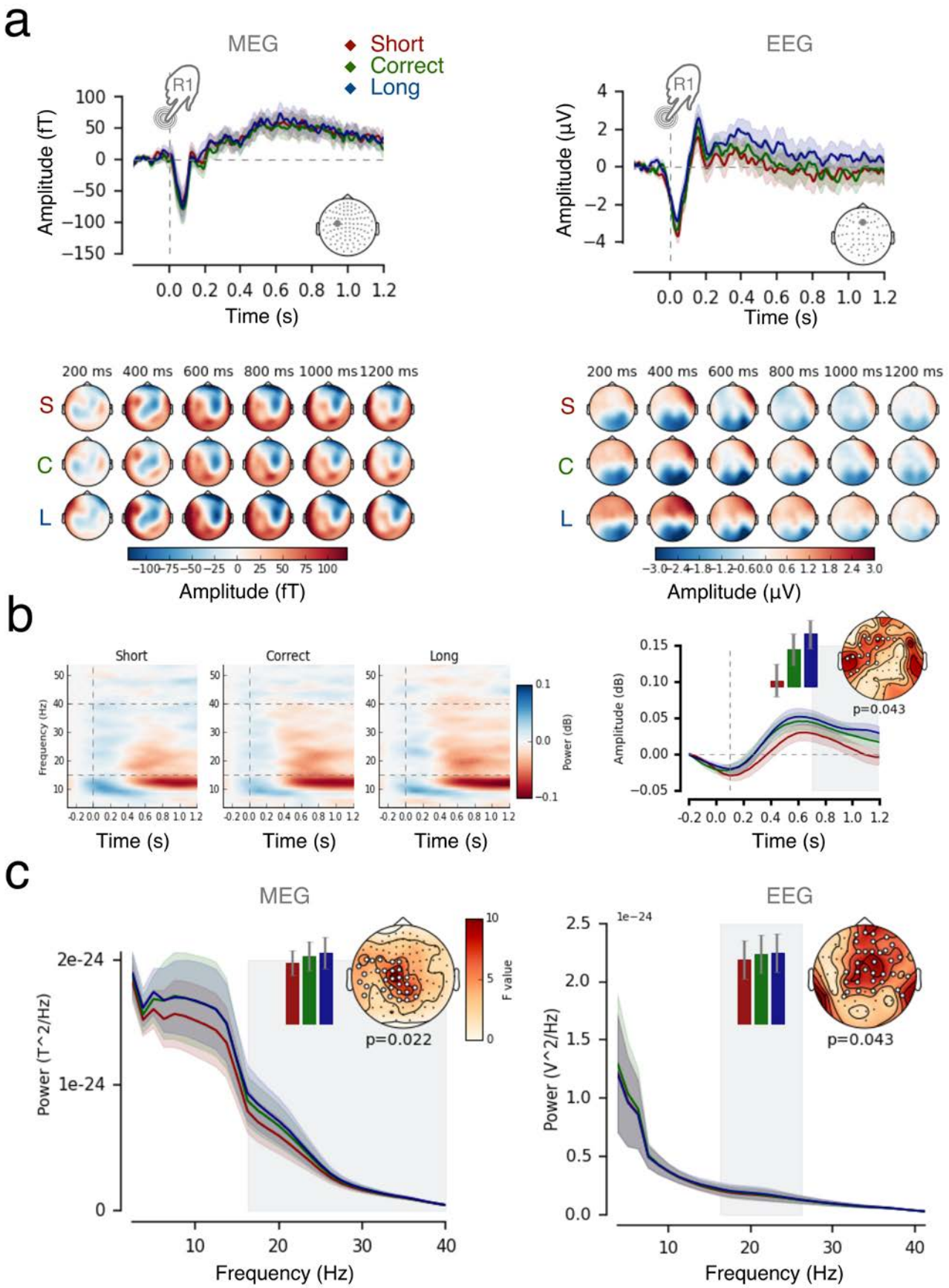

Supplementary Figure 2. β power controls FOJ as opposed to the slow brain activity. (**a**) Evoked ERP/F following the first keypress showed no significant effect as a function of FOJ for MEG and EEG (left and right panel, respectively). (**b**) The same time-frequency analysis in the same frequencies as those used for MEG analysis (15-40 Hz) confirmed the main observations derived based on MEG analysis, showing that larger values of β power yield longer duration production.

bioRxiv preprint doi: https://doi.org/10.1101/206086; this version posted October 19, 2017. The copyright holder for this preprint (which was not certified by peer review) is the author/funder, who has granted bioRxiv a license to display the preprint in perpetuity. It is made available under aCC-BY-NC-ND 4.0 International license.

(**c**) Power Spectrum Density (PSD) of MEG activity as a function of FOJ. Cluster-based permutation F-test on PSD estimates in the frequency dimension showed significant β (15-40 Hz) power increases as a function of longer duration productions for both MEG and EEG sensors. The significant frequency range is demarcated by vertical grey area. Topographical plot illustrates distribution of sensors included in the cluster. The barplot shows the averaged value in the significant region for all three FOJ conditions in the most significant sensor. EEG analysis, depicted in the right panel, confirmed observations obtained with MEG PSD spectrum for the example electrode.

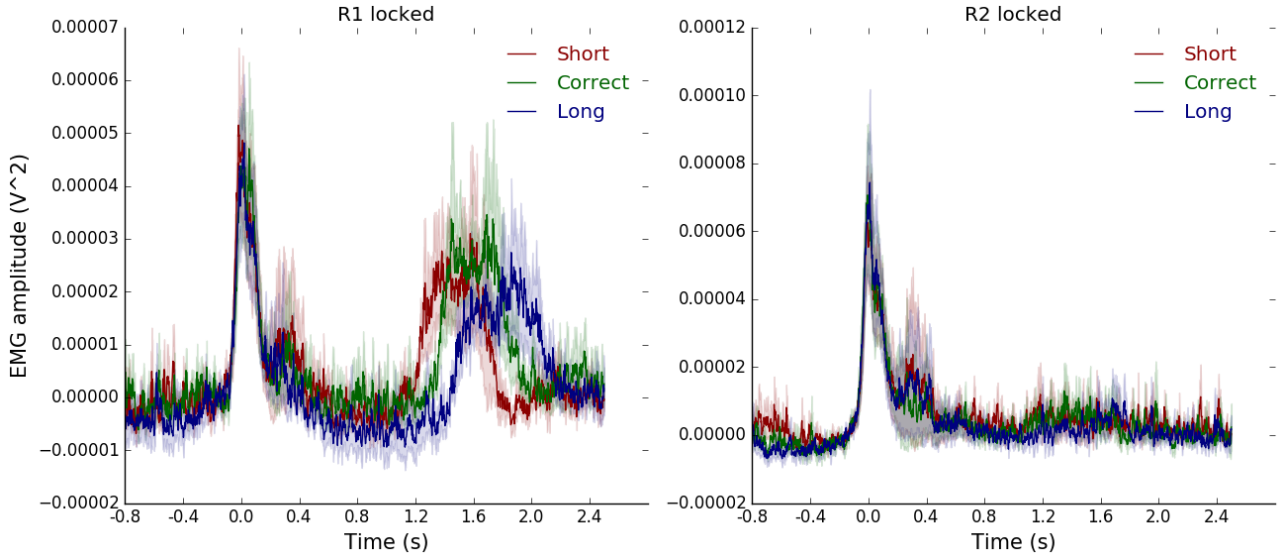

Supplementary Figure 3. Muscular activity does not impact FOJ. Both panels depict electromyographic (EMG) results. EMG recordings were split as a function of FOJ performance and time-locked to the first keypress. Differences across time production performance were tested using one way non-parametric Friedman's ANOVA in the 0 to 0.8 s time window following the first keypress with non-overlapping time windows of 0.1 s. The were no significant differences (R1-locked, all $p > 0.1$). The same analysis performed following the second keypress showed no significant differences between conditions (R2-locked, all $p > 0.1$). Overall, we found no evidence suggesting that motor activity could be a confounding factor for the main M/EEG findings.

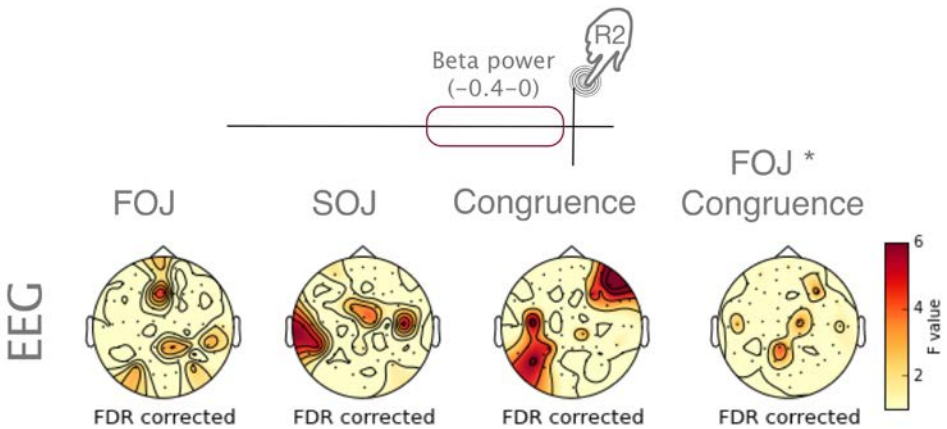

Supplementary Figure 4. GAMM model fits computed for β power in the 0.4 s time window preceding the second keypress. The topographical maps show that no significant effects were found, suggesting that the second key press is executed after β power reaches a certain fixed level.

bioRxiv preprint doi: https://doi.org/10.1101/206086; this version posted October 19, 2017. The copyright holder for this preprint (which was not certified by peer review) is the author/funder, who has granted bioRxiv a license to display the preprint in perpetuity. It is made available under aCC-BY-NC-ND 4.0 International license.

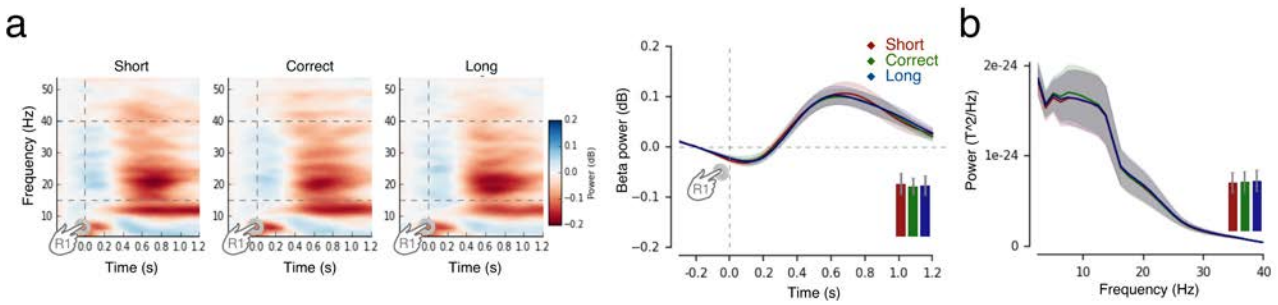

Supplementary Figure 5. (**a**) Time-frequency spectrum for the same MEG sensor as was used for the analysis based on the FOJ split. The β band is marked by horizontal grey lines. The results of cluster-based permutation F-test performed over time did not show any differences. No significant clusters were found (all $p > 0.1$). The barplot displays SOJ driven data using the same parameters as in FOJ driven condition. (**b**) The same SOJ based analysis for PSD values. Again MEG results of cluster-based permutation F-test of PSD estimates as a function of SOJ showed no effects in any frequency band. No significant clusters where also present for analogical analyses based on EEG data (all $p > 0.1$)

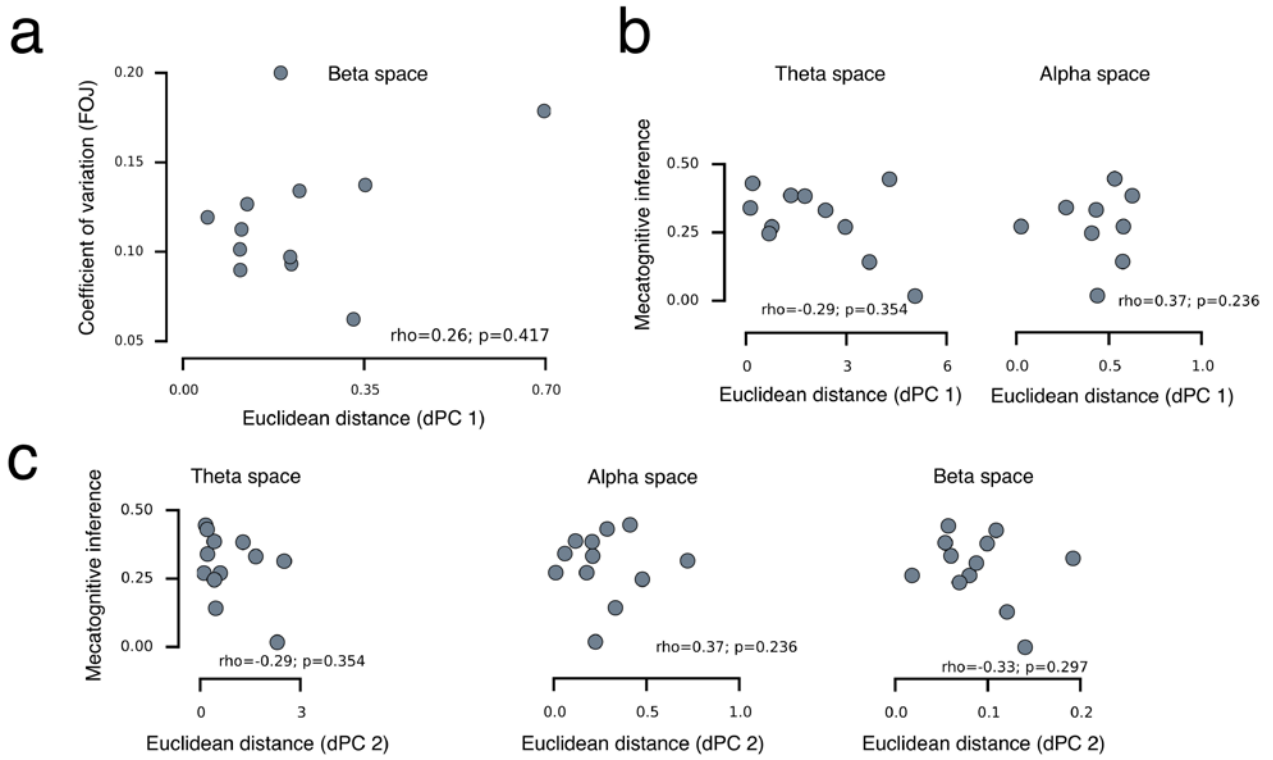

Supplementary Figure 6. (**a**) Individual distances in β state space (dPC 1) plotted against individual spread of FOJ (coefficient of variation). (**b**) Individual distances in theta and alpha state spaces (dPC 1) plotted against metacognitive inference (FOJ*SOJ). (**c**) Individual distances in theta, alpha, and β state spaces (dPC 2) plotted against metacognitive inference.

bioRxiv preprint doi: https://doi.org/10.1101/206086; this version posted October 19, 2017. The copyright holder for this preprint (which was not certified by peer review) is the author/funder, who has granted bioRxiv a license to display the preprint in perpetuity. It is made available under aCC-BY-NC-ND 4.0 International license.

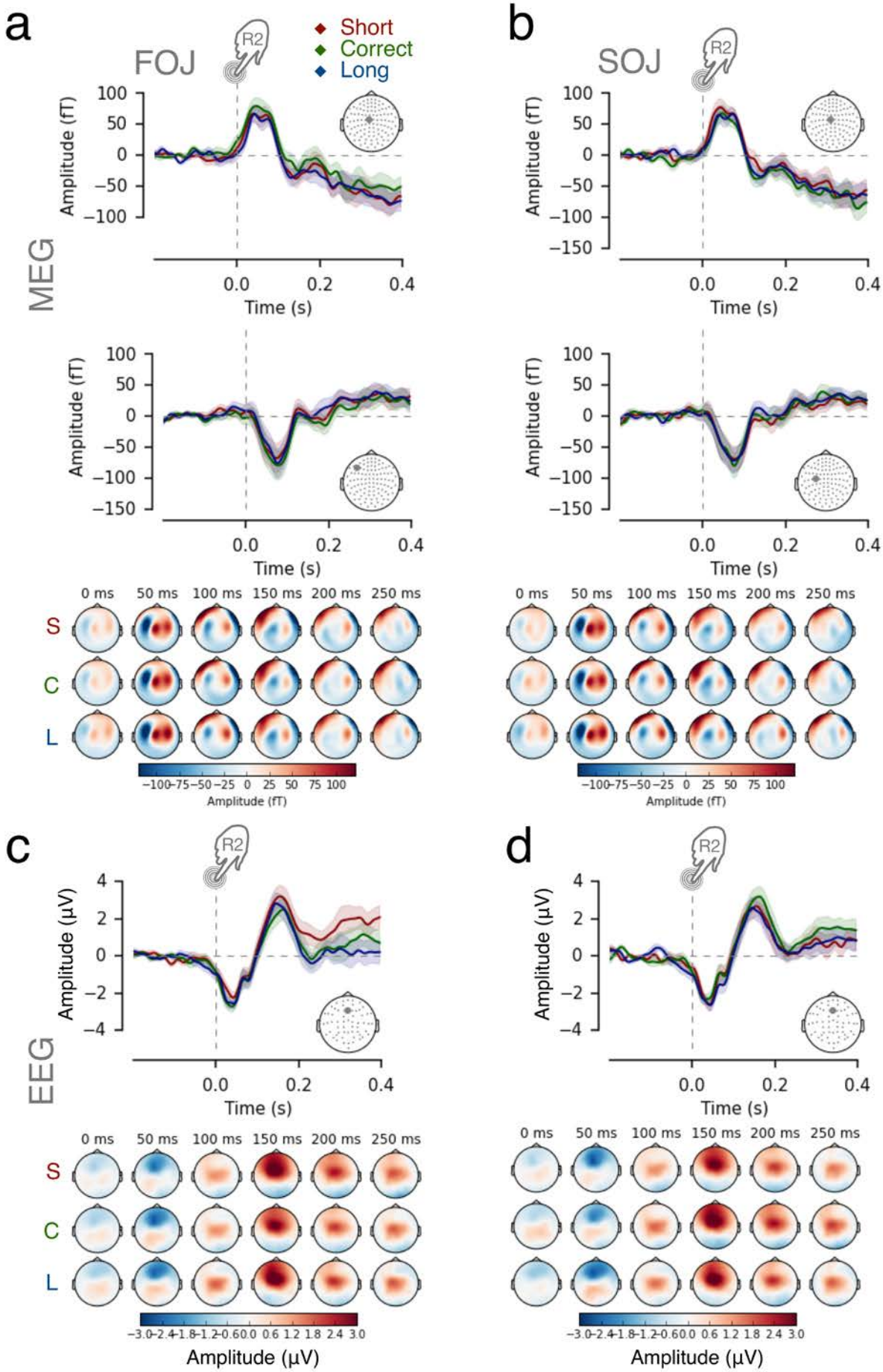

bioRxiv preprint doi: https://doi.org/10.1101/206086; this version posted October 19, 2017. The copyright holder for this preprint (which was not certified by peer review) is the author/funder, who has granted bioRxiv a license to display the preprint in perpetuity. It is made available under aCC-BY-NC-ND 4.0 International license.

Supplementary Figure 7. No ERN-like response. Evoked ERP/F up to 0.4s following the second keypress showed no significant effect as a function of FOJ or SOJ. Topographical plots in each panel illustrate time courses split according to FOJ or SOJ. Grey sensor maps illustrate which sensor displayed in a given panel. (**a**) MEG data split according to FOJ conditions. (**b**) MEG data split according to SOJ conditions. (**c**) EEG ('Fz') data split according to FOJ conditions. (**d**) EEG ('Fz') data split according to SOJ conditions.

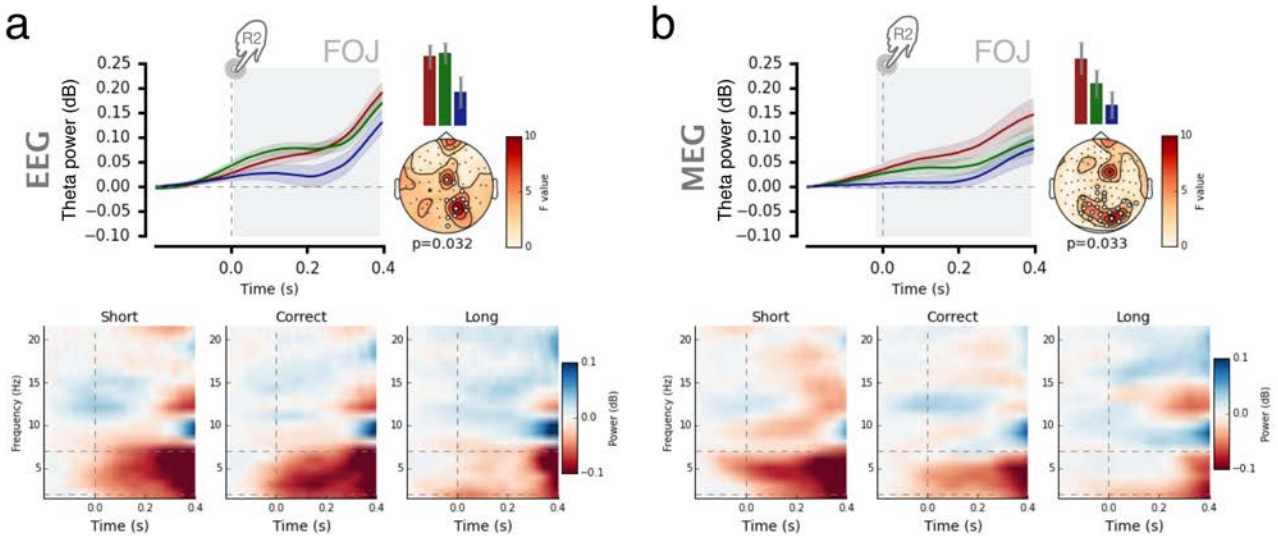

Supplementary Figure 8. Post-interval theta power contributes to temporal error-monitoring. (**a**) Results of theta power analyses following the second press. Cluster-based permutation test of time-frequency estimates based on the FOJ split for the EEG. The time courses illustrate 'short', 'correct', and 'long' FOJ conditions for the sensor with the highest F value. The bar plot illustrates relative difference of activity in the channel with the largest F value in the significant time window, depicted as shaded area in the time course plots. (**b**) Cluster-based permutation test of time-frequency estimates based on the FOJ split for the MEG data. Display is arranged analogically to panel 'a'.

bioRxiv preprint doi: https://doi.org/10.1101/206086; this version posted October 19, 2017. The copyright holder for this preprint (which was not certified by peer review) is the author/funder, who has granted bioRxiv a license to display the preprint in perpetuity. It is made available under aCC-BY-NC-ND 4.0 International license.

SUPPLEMENTARY TABLES

A. parametric coefficients	Estimate	Std. Error	t-value	p-value
(Intercept)	0.0008	0.0063	0.1346	0.8929
B. smooth terms	edf	Ref.df	F-value	p-value
s(FOJ)	1.0000	1.0001	26.5169	< 0.0001
s(SOJ)	1.0001	1.0002	0.0199	0.8877
s(Congruence)	1.0001	1.0002	6.4454	0.0111
ti(FOJ * SOJ)	1.5884	1.9788	0.8339	0.4507
ti(FOJ * Congruence)	1.0044	1.0088	8.0907	0.0044
s(subject)	0.0006	11.0000	0.0000	1.0000
GAMM analysis: R1-locked Beta power, FOJ cluster				

Supplementary Table 1. The results of single trial GAMM analysis based on beta power following the first keypress. The table displays the results for the final model that was based on the data collapsed across the significant sensors, showing the main effect of FOJ, when the model was fitted on per-sensor basis.

A. parametric coefficients	Estimate	Std. Error	t-value	p-value
(Intercept)	0.0012	0.0093	0.1274	0.8986
B. smooth terms	edf	Ref.df	F-value	p-value
s(FOJ)	3.9387	5.0159	5.0553	0.0001
s(SOJ)	1.0000	1.0001	15.0954	0.0001
s(Congruence)	1.0001	1.0002	1.1390	0.2859
ti(SOJ * FOJ)	2.2156	2.7321	1.2167	0.4324
ti(FOJ * Congruence)	1.0018	1.0036	17.0089	< 0.0001
s(subject)	0.0010	11.0000	0.0000	1.0000
GAMM analysis: R1-locked Beta power, FOJ * Congruence cluster				

Supplementary Table 2. The results of single trial GAMM analysis based on beta power following the first keypress. The table displays the results for the final model that was based on the data collapsed across the significant sensors, showing the interaction effect between FOJ and Congruence, when the model was fitted on per-sensor basis.

bioRxiv preprint doi: https://doi.org/10.1101/206086; this version posted October 19, 2017. The copyright holder for this preprint (which was not certified by peer review) is the author/funder, who has granted bioRxiv a license to display the preprint in perpetuity. It is made available under aCC-BY-NC-ND 4.0 International license.

A. parametric coefficients	Estimate	Std. Error	t-value	p-value
(Intercept)	-0.0009	0.0072	-0.1318	0.8951
B. smooth terms	edf	Ref.df	F-value	p-value
s(FOJ)	1.0001	1.0001	0.3260	0.5680
s(SOJ)	1.0002	1.0003	20.5239	< 0.0001
s(Congruence)	1.0002	1.0005	1.0091	0.3151
ti(SOJ * FOJ)	1.0027	1.0055	0.8087	0.3700
ti(FOJ * Congruence)	1.0089	1.0178	1.3847	0.2368
s(subject)	0.0015	11.0000	0.0000	0.9948
GAMM analysis: R2-locked Sustained activity, Anterior cluster				

Supplementary Table 3. The results of single trial GAMM analysis based on sustained activity preceding the second keypress. The table displays the results for the final model that was based on the data collapsed across the significant sensors, showing the main effect SOJ, when the model was fitted on per-sensor basis. The table depicts the anterior cluster.

A. parametric coefficients	Estimate	Std. Error	t-value	p-value
(Intercept)	-0.0040	0.0074	-0.5389	0.5900
B. smooth terms	edf	Ref.df	F-value	p-value
s(FOJ)	1.0000	1.0001	0.1091	0.7412
s(SOJ)	1.0000	1.0001	27.6527	< 0.0001
s(Congruence)	1.0000	1.0001	4.4611	0.0347
ti(SOJ * FOJ)	2.0365	2.5519	1.3882	0.2115
ti(FOJ * Congruence)	1.0077	1.0153	1.0731	0.2974
s(subject)	0.0003	11.0000	0.0000	0.9815
GAMM analysis: R2-locked Sustained activity, Posterior cluster				

Supplementary Table 4. The results of single trial GAMM analysis based on sustained activity preceding the second keypress. The table displays the results for the final model that was based on the data collapsed across the significant sensors, showing the main effect SOJ, when the model was fitted on per-sensor basis. The table depicts the posterior cluster.

A. parametric coefficients	Estimate	Std. Error	t-value	p-value
Intercept	0.0006	0.0078	0.0810	0.9355
FOJ	-0.0474	0.0107	-4.4482	< 0.0001
B. smooth terms	edf	Ref.df	F-value	p-value
ti(FIJ * Congruence)	1.0016	1.0032	2.8503	0.0913

bioRxiv preprint doi: https://doi.org/10.1101/206086; this version posted October 19, 2017. The copyright holder for this preprint (which was not certified by peer review) is the author/funder, who has granted bioRxiv a license to display the preprint in perpetuity. It is made available under aCC-BY-NC-ND 4.0 International license.

s(Congruence)	1.0007	1.0013	0.0125	0.9122
s(SOJ)	1.0003	1.0006	0.7253	0.3946
s(subject)	0.0031	11.0000	0.0000	1.0000
GAMM analysis: R2-locked Alpha power, FOJ cluster, full model				

Supplementary Table 5. The results of single trial GAMM analysis based on alpha power following the second keypress. The table displays the results for the final model that was based on the data collapsed across the significant sensors, showing the main effect FOJ, when the model was fitted on per-sensor basis.

A. parametric coefficients	Estimate	Std. Error	t-value	p-value
Intercept	0.0033	0.0078	0.4175	0.6763
B. smooth terms	edf	Ref.df	F-value	p-value
ti(FOJ * Congruence)	1.0016	1.0033	0.3603	0.5491
s(Congruence)	1.0007	1.0013	0.0004	0.9854
s(SOJ)	1.0001	1.0002	12.1300	0.0005
s(subject)	0.0012	11.0000	0.0000	0.9999
GAMM analysis: R2-locked Alpha power, SOJ cluster, Model without FOJ term				

Supplementary Table 6. The results of single trial GAMM analysis based on alpha power following the second keypress. The table displays the results for the final model that was based on the data collapsed across the significant sensors, showing the main effect SOJ, when the model was fitted on per-sensor basis and the FOJ term has been excluded from the model.